Physicochemical characterization of Portuguese clay and nanocomposite preparation with polylactide

Chih-Te Huang

Thesis submitted to the

Faculty of Graduate and Postdoctoral Studies

in partial fulfillment of the requirements

For the MSc degree in Chemistry

Department of Chemistry

Faculty of Science

University of Ottawa

Acknowledgements

I would like to say thank you to my supervisor: Professor Christian Detellier for giving me opportunities to complete this master thesis and supporting me all the way.

I would like to express my special gratitude to Rola Mansa, who organized everything for me and reviewed my thesis draft several times, to Dr. Gustave Kenne, who is like my brother and always patiently teach me everything, to Anna Czarnecka for the beneficial discussions and the company to fight the experiments, and other members in Detellier's group for their assistance.

I would like to thank Professor Fernando Rocha for his arrangement in Portugal and providing experienced knowledge of clay, and all the members and classmates in Aveiro especially Wondemagegn Wanna, Tang Ruini, Catia Curie and Stanislav Jelavić for their help in experiments and life.

I would like to give my deep appreciation to the IMACS committee for providing this amazing opportunity to me and especially thank you to Professor Patricia Patrier and Sophie Levesque for their caring during the whole study journey.

I would like to thank my examiners for reading my thesis and giving me many constructive suggestions.

The last but the most important gratitude is to my parents, who support and encourage me all the time.

Abstract

A Portuguese clay (BRN) from the North East city of Bragança was collected and characterized in terms of health treatment and applied towards the preparation of nanocomposites with Polylactide (PLA). The silt-clay fraction of BRN is mainly composed of smectite with less illite, kaolinite and other minerals. The physicochemical properties are applicable for the topical applications and are mainly influenced by smectite. With the hazardous elements present, further bioavailability tests should be conducted. PLA nanocomposites with BRN and Wyoming montmorillonite SWy-2 (MMT) were respectively prepared through the solution casting method with ultrasonic stirring and using cetyltrimethylammonium bromide (CTAB) as the surfactant. The X-ray diffraction patterns show the exfoliated structures in most samples. Thermal gravimetric analysis reveals the increased thermal stability of the nanocomposites. The complexes were also characterized by nitrogen adsorption, infrared analysis and nuclear magnetic resonance for comparing the differences between BRN and MMT.

Table of Contents

Abbreviation

^{o}C	degree Celsius
µm	micrometer
BRN	Portuguese clay- Bragança sample
BRN3%/PLA	the blending of 97% polylactide with 3% Bragança sample
CEC	cation exchange capacity
CTA	cetyltrimethylammonium ion
CTAB	cetyltrimethylammonium bromide
DTG	derivative thermogravimetry
et al.	Latin: Et alii which means and others
Eds.	editors
fig.	figure
IR	infrared analysis
LL	liquid limit
LOI	loss on ignition
mol	mole
m-MMT	montmorillonite modified by cetyltrimethylammonium ion

m-BRN3%/PLA	the blending of 97% polylactide with 3% Bragança sample which is modified by cetyltrimethylammonium ion
m-MMT3%/PLA	the blending of 97% polylactide with 3% montmorillonite which is modified by cetyltrimethylammonium ion
MMT3%/PLA	the blending of 97% polylactide with 3% montmorillonite
PL	plastic limit
PI	plastic index
rpm	revolutions per minute
SWy-2	montmorillonite from Wyoming, USA
TEM	transmission electron microscopy
TGA	thermogravimetric analysis
wt.%	weight percentage
XRD	x-ray diffraction

List of Figures and Tables

Chapter 1 : Introduction

1.1 Structure and properties of clay minerals

Clays and clay minerals, the most important materials of the 21st century, are abundant, inexpensive and environmentally friendly (Bergaya & Lagaly, 2006). Clay has been known to, and used by, humans since antiquity. In modern times, it is still a required material in many ceramic products such as porcelain, bricks, tiles and sanitary ware as well as an important additive in plastics, paints, paper, rubber and cosmetics. Clay is non-polluting and can also be a depolluting agent. In the near future, the most likely development is to modify the properties of polymer by dispersing clay in polymer, forming a nanocomposite (Bergaya & Lagaly, 2006).

According to the definition made by the joint nomenclature committees (JNCs) of the Association Internationale pour l'Etude des Argiles (AIPEA) and the Clay Minerals Society (CMS), clay is a naturally occurring material composed primarily of fine-grained minerals, which are generally plastic at appropriate water contents and will harden when dried or fired (Guggenheim & Martin, 1995). The particle size of clay is less than 2 μm (Pinnavaia, 1983). In the engineering industry, plasticity is measured by the plasticity index which is the water content between liquid and plastic limit. According to the empirical rule, when the plastic index (PI) is greater than 25%, it would easily expand and swell when getting wet. In industry, the practical clay can

be divided into four types: (1) bentonite which is mainly composed of montmorillonite, (2) kaolins, (3) palygorskite and sepiolite, and (4) the clay with illite/smectite structure used in ceramics (Bergaya & Lagaly, 2006).

The distinctions between clays and clay minerals are listed on Table 1.1. The word clay is mainly used for the rock term and in geology, while clay mineral refers to the mineral term. The main properties of clay minerals are: (1) Nano-scale in one dimension. (2) Anisotropy of layer and particle. (3) With external basal (planar), edge and internal (interlayer) surface (4) Modification by adsorption, ion exchange and grafting on external and internal surface. (5) Plasticity. (6) Generally, hardening when drying and firing. (Bergaya & Lagaly, 2006).

Clay	Clay mineral
Natural	Natural and synthetic
Fine-grained (<2μm or <4μm)	No size criterion
Phyllosilicates as principal constituents	May include non-phyllosilicates
Plastic	Plastic
Hardens on drying or firing	Hardens on drying or firing

Table 1.1 Distinction between clay and clay mineral (Bergaya & Lagaly, 2006).

Clay minerals are hydrous aluminum layered silicates (Meunier, 2005) consisting of tetrahedral sheets and octahedral sheets which are continuous in two dimensions. The layer which is the unit of different clay minerals, was composed of sheets in different ways. The particles, made up of layers, form aggregates as shown by Figure 1.1. The chemical formula of the tetrahedral sheet is T_2O_5 of which T is a tetrahedral cation, mainly Si^{4+}, Al^{3+}, Fe^{3+} (Brigatti *et al.*, 2006) and rarely Be^{2+} and B^{3+}. One tetrahedron is composed of four oxygens, coordinated with T, three basal ones which are shared with adjacent tetrahedra forming the hexagonal mesh pattern. The fourth one in the apical corner usually points in the normal direction with sheets and forms part of the octahedral sheet. In the center of the octahedral, there are mid-sized cations, usually Al^{3+}, Mg^{2+}, Fe^{2+} and Fe^{3+}. The individual octahedra are linked by sharing oxygen and edges with adjacent octahedra and are vertically connected with the tetrahedra. One unit of the octahedral sheet is composed of three octahedra. Some oxygens existing in the hydroxyl form makes phyllosilicates with a charge deficiency, which is balanced by different cations, water and other molecules (Brown *et al*. 1984).

Phyllosilicates can be divided into two forms: one is the 1:1 layer which is composed of one tetrahedral sheet with one octahedral sheet, the thickness of which usually is 0.7nm. Another is the 2:1 layer, which is one octahedral sheet sandwiched by two tetrahedral sheets and the thickness is 1nm, which is shown as Figure 1.2

(Bhattacharya & Gupta, 2008). The lateral dimension can be varied from 30nm to several microns or even larger.

Montmorillonite is a member of the smectite group. According to the different exchangeable cations within the interlayer, there are different types of smectites. The most important one in industry is Na-montmorillonite (Murray, 2000). The layer of smectite is formed by one octahedral sheet sandwiched by two tetrahedral sheets and belonging to the 2:1 layer type of clay mineral. There are van der Waals forces between layers. With isomorphic substitution, the Si^{4+} of the tetrahedral sheet is replaced by an Al^{3+}, while the Al^{3+} in the octahedral sheet is replaced by a Mg^{2+} causing negative charge and neutralized by exchangeable ions such as K^{+}, Na^{+}, Ca^{2+} and Mg^{2+}(Ray & Okamoto, 2003). Those exchangeable cations are hydrous and are easily replaced by other cations and organic molecules, thus expanding the interlayer space along the c direction making montmorillonite a suitable material for preparing nanocomposites (Ray & Okamoto, 2003). This property can be measured by the cation exchange capacity (CEC) which is the ability of the clay mineral to adsorb cations from solution. However it is not constant, but depends on the layer. Therefore, it can be considered as the average of the whole crystal (Ray & Okamoto, 2003). In a pristine clay mineral, there are only hydrous cations, such as sodium and potassium within the interlayer, which can interact with hydrophilic polymers like poly(ethylene

oxide) (PEO), poly(vinyl alcohol) (PVA) (Ray & Okamoto, 2003). In order to be possibly miscible with more polymers, the surface of clay minerals can be modified from hydrophilic to organophilic by cationic surfactants such as primary, secondary, tertiary, and quaternary alkylammonium or alkylphosphonium cations, which can lower the surface energy and improve the wetting characteristics of the polymer matrix to enlarge the interlayer spacing. Moreover, these surfactants can provide functional groups to interact with the polymer matrix or in certain conditions, polymerize the monomer to increase the adhesion between inorganic and polymer matrix (Ray & Okamoto, 2003).

Through the chemical composition analysis, the sample used in this study mainly contains smectite, with less kaolinite and illite of which the structure and properties are to follow.

Kaolinite is a member of the kaolin group which has a 1:1 layer type composed of one tetrahedral sheet and one octahedral sheet whose chemical formula is $Al_2Si_2O_5(OH)_4$, same as the other two members, dickite and nacrite. In comparison, the other member of the kaolin group, halloysite, has the chemical formula $Al_2Si_2O_5(OH)_4 \cdot 2H_2O$. It has water inside the interlayer space, and its sructure can be spheres, tubes, plates and laths. Now many researchers are focused on the application of kaolinite and trying to make nanocomposites (Brigatti *et al*., 2006).

Illite belongs to the mica group and is a 2:1 layer clay, same as smectite. The difference between them is the main interlayer cation. The one in illite is potassium which fits to the oxygen of tetrahedra because of the size, charges, and coordinates forming the ionic bonds making the layers compact and preventing water molecules from entering into the interlayer. Therefore, it is not appropriate for making the nanocomposite (Murray, 2007).

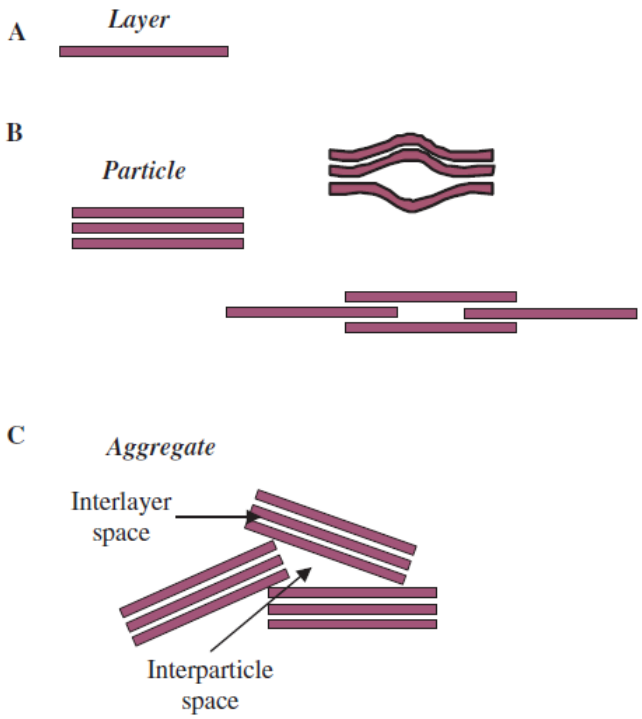

Figure 1.1 (A) a clay mineral layer (B) a particle (C) an aggregate (Bergaya & Lagaly, 2006).

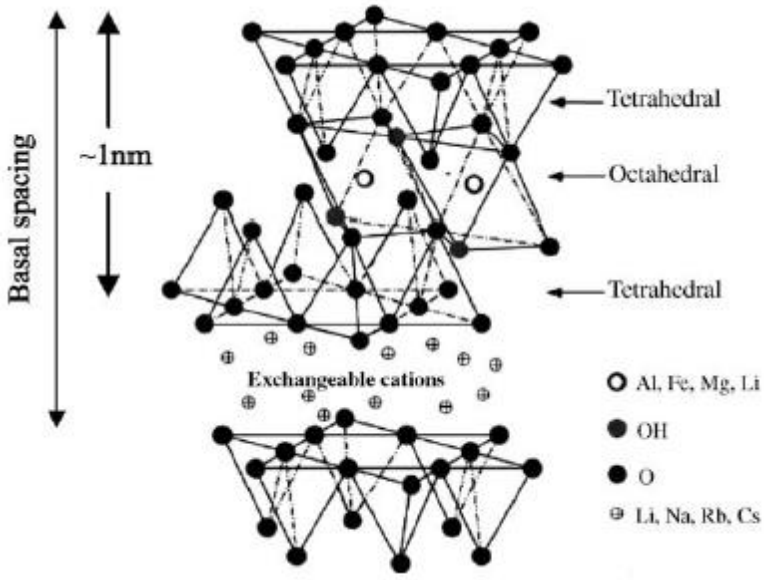

Figure 1.2 Structure of 2:1 phyllosilicates (Ray & Okamoto, 2003).

1.2 Clay minerals for human health

The usage of clay minerals for human health has a long history. In the prehistoric period, Homo Erectus and H. Neanderthalensis used several clay minerals mixed with water to cure wounds, sooth irritation and clean skin. The Greeks used clay as an antiseptic cataplasm which is a poultice and to cure snake bites. Marco Polo also described the phenomenon when Muslim pilgrims ingested “pink earth” to cure fevers. Chinese references about the curative clays appear in Pen Ts’ao Kang Mu which is a famous old catalogue about Chinese medicine (Carretero *et al*., 2006).

The clay minerals used in pharmaceutical formulations are mainly smectite, palygorskite, kaolinite and talc. The required properties for such clay minerals are high specific surface area, high adsorption capacity, high rheology, chemical inertness and low or null toxicity (Carretero, 2002). They can be considered as both active principles and excipients. As active principles, depending on the application, the use of clay minerals can be divided into oral and topical applications. For oral applications, they can be used as gastrointestinal protectors, laxatives and anti-diarrhoea agents (Carretero, 2002). As gastrointestinal protectors, the clay minerals adhere to the gastric and intestinal mucous membrane to absorb toxins, bacteria and viruses. However, the disadvantage is that they also eliminate enzymes and other nutritive elements. Therefore, the long term use is not suggested. The way

they are eliminated from the body is through the faeces because these minerals are not absorbed by the intestinal tract and are not easily soluble in aqueous media (Carretero, 2002).

When used in topical applications, clay minerals can be applied to the body's exterior as dermatological protectors and cosmetics. When used as dermatological protectors, they are usually in powder, cream and ointment types to form a film which protects skin from physical and chemical agents. In cosmetics, they can be applied as face masks due to their high absorbency of unfavorable substances such as greases and toxins. As excipients, the use of clay minerals is to improve three factors: (1) taste, smell and color, (2) the preparation of pharmaceutical formulation, and (3) the disintegration of the pill (Carretero, 2002).

Clay minerals for healing purpose are mostly used in spas. They can be mixed with water for geotherapy, and with sea and salty lake water or mineral water as pelotherapy or mixed with paraffin as paramud. The most useful clay minerals for this purpose are smectite and kaolinite, although illite and palygorskite are occasionally used. They are applied alone or served with other clay minerals. The main properties for use in spas are the adsorption capacity, high cation exchange capacity, plasticity, rheology, particle size and cooling rate (Carretero, 2002). On the other hand, it is necessary to study the existence of hazardous elements such as As, Pb, Hg, Cd, Se, Sb,

Cu, Zn, etc. and their mobility to prevent harmful effects to health. The geotherapy uses can be divided into cataplasms for a small area of the body and mud baths for the whole body. Both are used to treat dermatological diseases such as boils, acne, ulcers, abscess and seborrhoea and to alleviate the pain caused by chronic rheumatic inflammations and sport traumatism. The temperature of the geotherapy application depends on the therapeutic aims. The pelotherapy and paramuds are generally applied hot between 40-45^{o}C (Carretero, 2002).

1.3 Polylactide

Polylactide (PLA) is a linear aliphatic polyester with biodegradable and biocompatible properties made from renewable resources like corn, sugar beets or rice (Fig.1.3) (Marras et al., 2007; Vink et al., 2003). It has shown to be the most promising biodegradable polymers in medical applications due to its relatively strong mechanical properties. Polylactide has been successfully used for many medical implants such as pins, rods, screws, and anchors, and is approved by regulatory agencies in many countries (Suzuki & Ikada, 2010). In terms of packaging and container, oriented polylactide film is transparent and tough with reasonable thermal and impact resistance and can be applied on vegetable bags, transparent envelope windows, laminated paper bags and so on (Obuchi & Ogawa, 2010).

Polylactide does not exist in nature. The manufacturing of polylactide from lactic acid was pioneered by Carothers in 1932. However this product was of a low molecular weight with poor mechanical properties. Afterwards, DuPont produced a higher molecular weight polylactide in 1954. Due to the high cost of producing polylactide, the application is only focused on the biomedical purpose. In the late 1980s, advances in bacterial fermentation of D-glucose from corn decreased the cost of the product and improved the potential of non-medical use (Lunt, 1998).

The conversion of lactic acid to polylactide is achieved either by direct

condensation of lactic acid or by the ring-opening polymerization of the cyclic lactide dimer (Marras *et al*., 2007). The direct condensation path is an equilibrium reaction with difficulties in removing water and only producing low to intermediate molecular weight polylactide. However, Mitsui Toatsu Chemicals developed and patented a new direct condensation process to produce high molecular weight Polylactide (Marras *et al*., 2007; Vink *et al*., 2003). On the other hand, Cargill Dow LLC developed the ring-opening polymerization which can produce high molecular weight polylactide. In the first step of the process water is removed to produce a low molecular weight prepolymer. This prepolymer is then catalytically depolymerized to form cyclic lactide dimer which is then purified by distillation. The purified lactide is polymerized in a solvent free ring-opening polymerization. The process of the ring-opening polymerization is shown in Figure 1.4 (Vink *et al*., 2003).

Because there are four unique groups attached to the central carbon atom, lactic acid is a chiral molecule which has two stereoisomer “L” and “D” which are shown in Figure 1.5 (Vink *et al*., 2003). The production of the cyclic lactide has three forms: the D-lactide, L-lactide and meso lactide shown as Figure 1.6 (Vink *et al*., 2003). Polylactide with high L-lactide levels are more crystalline which affects the mechanical and biodegradable properties (Vink *et al*., 2003). As a consequence, polylactide can display a range of glass transition temperatures from 50^{o}C to 80^{o}C and

a range of melting points from 130°C to 180°C (Marras *et al*., 2007).

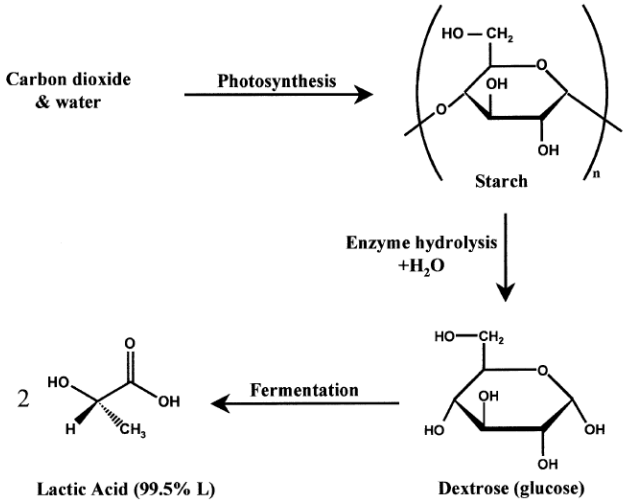

Figure 1.3 The overview of lactic acid manufacturing (Vink et al., 2003).

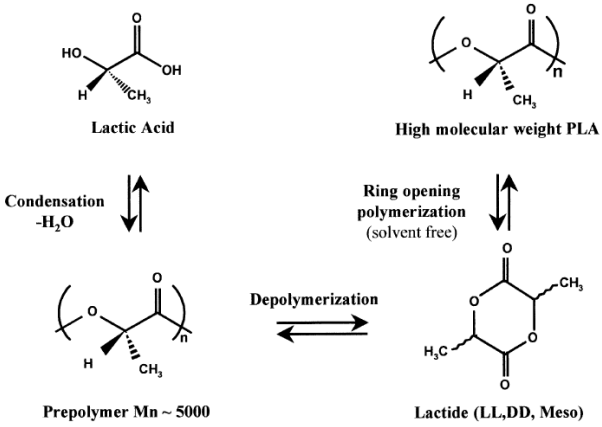

Figure 1.4 The overview of PLA manufacturing (Vink et al., 2003).

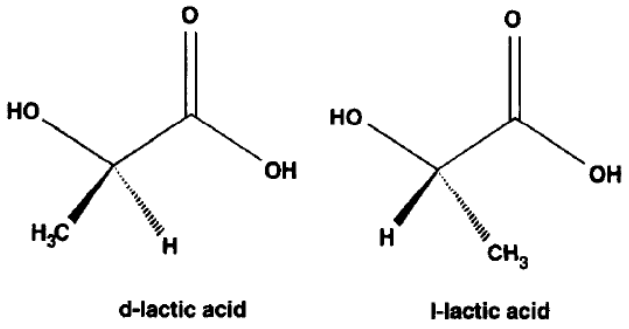

Figure 1.5 Two stereoisomers of lactic acid (Lunt, 1998).

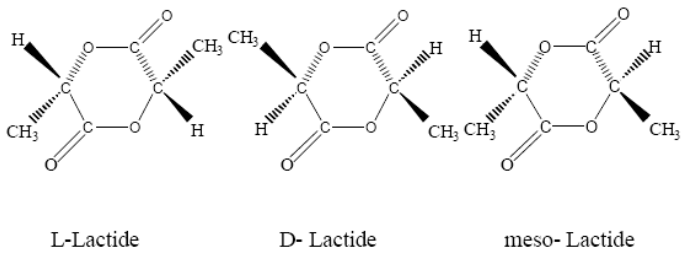

Figure 1.6 Three stereoisomers of lactide (Chiang, 2011).

1.4 Conclusion and objectives

In this thesis, Portuguese clay (BRN) plays a main role. In order to discover the potential applications of it, we focused on two fields- healing applications and the nanocomposite preparation with polylactide (PLA), the promising biodegradable polymer.

Through the reviews of chapter 1.1, the most important concept is the structure and the properties of smectite which is the main component in BRN. It belongs to 2:1 layer clay minerals and has swelling property. The hydrous cations within interlayer of smectite can be exchanged by organic ions to modify smectite from hydrophilic to organophilic which is the main mechanism for the nanocomposite preparation. Chapter 1.2 reviews the healing applications of clay minerals. The most applicable clay mineral is smectite which has high specific surface area and adsorption capacity. The hazardous elements of materials should be noticed. The industrial applications of PLA are described in chapter 1.3. The medical implants of PLA can be bound with the healing minerals. And those nanocomposites could increase the properties of PLA.

In this experiment, we analyzed the BRN according to the required properties for the healing application and attempted the nanocomposites synthesis.

Reference

Bergaya, F. & Lagaly, G. (2006). General introduction: clays, clay minerals, and clay science. In F. Bergaya, B.K.G. Theng and G. Lagaly (Eds.), *Handbook of Clay Science* (pp.1-18). Amsterdam: Elsevier Science.

Bhattacharya, K. G. & Gupta, S. S. (2008). Adsorption of a few heavy metals on natural and modified kaolinite and montmorillonite: A review. *Advances in Colloid and Interface Science, 140*(2), 114-131.

Brigatti, M. F., Galan, E., & Theng, B. K. G. (2006). Structures and mineralogy of clay minerals. In F. Bergaya, B. K. G. Theng & G. Lagaly (Eds.), *Handbook of Clay Science* (pp. 19-85). Amsterdam: Elsevier Science.

Brown, G. (1984). Crystal Structures of Clay Minerals and Related Phyllosilicates. *Phil. Trans. R. Soc. Lond. A311*, 221-240.

Carretero, M. I. (2002). Clay minerals and their beneficial effects upon human health. A review. *Applied Clay Science, 21*(3-4), 155–163.

Carretero, M. I., Gomes, C.S.F. & Tateo, F. (2006). Clays and human health. In F. Bergaya, B.K.G. Theng and G. Lagaly (Eds.), *Handbook of Clay Science* (pp.717-741). Amsterdam: Elsevier Science.

Chiang, Ming-Feng (2011). Preparation and Pyrolysis Behaviors of Poly(L-lactide)/Layered Double Hydroxide Nanocomposites. (Master thesis)

pp.13.

Guggenheim, S. & Martin, R. T. (1995). Definition of clay and clay mineral: joint report of the AIPEA nomenclature and CMS nomenclature committees. *Clays and Clay Minerals 43*, 255-256.

Lunt, J. (1998). Large-scale production, properties and commercial applications of polylactic acid polymers. *Polymer Degradation and Stability, 59* (1-3), 145-152.

Marras, S. I., Zuburtikudis, I. & Panayiotou, C. (2007). Nanostructure vs. microstructure: Morphological and thermomechanical characterization of poly(L-lactic acid)/layered silicate hybrids. *European Polymer Journal, 43* (6), 2191–2206.

Meunier, A. (2005) *Clays* (pp.472). Springer-Verlag Berlin Heidelerg, Germany.

Murray, H. H. (2000). Traditional and new applications for kaolin, smectite, and palygorskite: A general overview. *Applied Clay Science, 17*(5-6), 207-221.

Murray, H. H. (2007). *Applied clay mineralogy occurrences, processing, and application of kaolins, bentonites, palygorskite-sepiolite, and common clays* (pp.15). Amsterdam ; Boston : Elsevier.

Obuchi, S. & Ogawa, S. (2010). Packaging and other commercial applications. In Auras, R. (Eds.), *Poly(lactic Acid): Synthesis, Structures, Properties, Processing, and Applications* (pp.457-467). Hoboken, N.J.: Wiley.

Pinnavaia, T. J. (1983). Intercalated clay catalysts. *Science*, *220*(4595), 365-371.

Ray, S. S. & Okamoto, M. (2003). Polymer/layered silicate nanocomposites: a review from preparation to processing. *Prog. Polym. Sci., 28,* 1539–1641.

Suzuki, S. & Ikada, Y. (2010). Medical applications. In Auras, R. (Eds.), *Poly(lactic Acid): Synthesis, Structures, Properties, Processing, and Applications* (pp. 445-456). Hoboken, N.J.: Wiley.

Vink, E.T.H., Rabago, K.R., Glassner, D.A. & Gruber, P.R. (2003). Applications of life cycle assessment to Nature Works™ polylactide (PLA) production. *Polymer Degradation and Stability, 80* (3), 403–419.

Chapter 2 : Major Techniques of Characterization

2.1 X-ray diffraction

X-ray methods are very common techniques to analyze the composition of the materials. X-rays are the electromagnetic radiation, according to quantum theory, which have wave-particle duality (Mark & Rex, 2013). The wavelength of x-rays range from 10 to 10^{-3} nm and their energy ranges from 100eV to 10MeV. X-rays were discovered by German physicist Wilhelm Conrad Röntgen in 1895 (He, 2009). Afterwards, the idea that a crystal can be the diffraction grating was proposed by Paul Peter Ewald and Max von Laue. Since the order of magnitude of wavelength is larger than the spacing in crystals, visible light as the diffraction source cannot reflect from crystal. On the contrary, Laue successfully used x-ray for the diffraction which has the same order of magnitude of wavelength with spacing in crystals. In 1912, William Lawrence Bragg and his father William Henry Bragg formulated Bragg's law $n\lambda=2d\sin\theta$ which is the significant equation to build the relation of diffraction. When the wavelength of radiation is close to the spacing between the atoms, the atoms can be considered as the diffraction grating and have the constructive and destructive interference of the scattering which is shown in Figure 2.1. The incident beam a and b have the same incident angle and travel distance which causes the constructive

interference. The incident beam c moves in phase with a and b if the extra travel distance 2dsinθ is equal to the integral number of wavelength, or it results in destructive interference when out of phase (Yoshio *et al*., 2011).

The constituents of an x-ray diffractometer are the source, sample, monochromater, detector and output device. In the hot cathode tube, the electrons are emitted from tungsten filament when heated, and travel through the electron field to impinge anode. There are two phenomena that happen when the impingement occurs. One is the inelastic collision when the partial kinetic energy of electron transfers into the continuous spectrum which is also called white radiation. Another is the characteristic spectrum which is caused by the excitation of the inner-shell electron with collision and meanwhile, the outer-shell electron fills the inner-shell and releases energy between the energy levels in x-ray form. The source of the x-ray diffractometer has a characteristic radiation, usually using Cu Kα and filtered by nickel as the monochromater, the wavelength of which is 1.5418Å (Mark & Rex, 2013).

The sample is mounted for the measurement and held in the x-ray beam passage and rotated. The detector is working as the film or charge-coupled device to record the pattern of spots or reflection. Afterwards, the output device assesses the collected data (He, 2009).

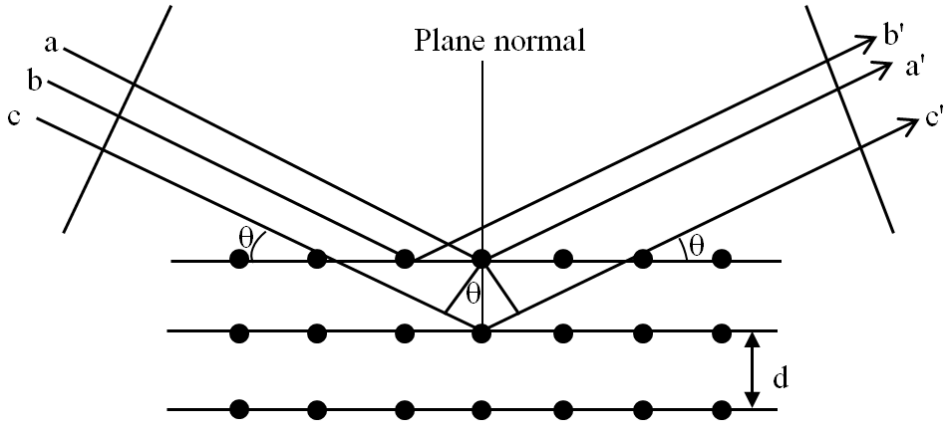

Figure 2.1 X-ray diffraction from a layered structure (Adapted from Yoshio et al., 2011).

2.2 Transmission electron microscopy

The transmission electron microscopy (TEM) is an essential instrument to diagnose materials. The historical development of TEM is from the discovery of the electron by J. J. Thomson in 1897 and the fact that electron beams could be deflected and concentrated through electrostatic and magnetic fields. In 1924, Louis de Broglie revealed the hypothesis that the electrons travel in a waveform pattern and derived the formula ($\lambda=h/mv$) where h is Planck's constant, m is the mass of a particle and v is the velocity of a particle. Afterwards, Ernst E. Ruska developed the magnetic lens and built the first TEM in 1931 (Gunning & Calomeni, 2000).

The TEM can provide information on several properties of the material studied including morphology, structure, lattice imaging and chemical composition (Elsass, 2006). The TEM can be divided into three components: the illumination system, the objective lens/specimen stage, and the imaging system. The illumination system, consisting of the gun and the condenser lenses, emit the electrons from the heated filament. They are accelerated by a potential difference and passed through a set of condenser lenses to limit the desired diameter. The illumination system can be operated in two principal modes: parallel beam and convergent beam. The objective lens and the sample stage system is the heart of the TEM where the electron beams penetrate the ultrathin specimen and cause all of the interactions (Fig. 2.2). The lenses

of the imaging system magnify the electron intensity distribution and focus on a fluorescent screen. The image can be recorded by direct exposure of a photographic emulsion or an image plate inside the vacuum or digitally via a fluorescent screen coupled by a fiber-optic to a charge-coupled device (CCD) (Williams & Carter, 2009; Reimer & Kohl, 2008).

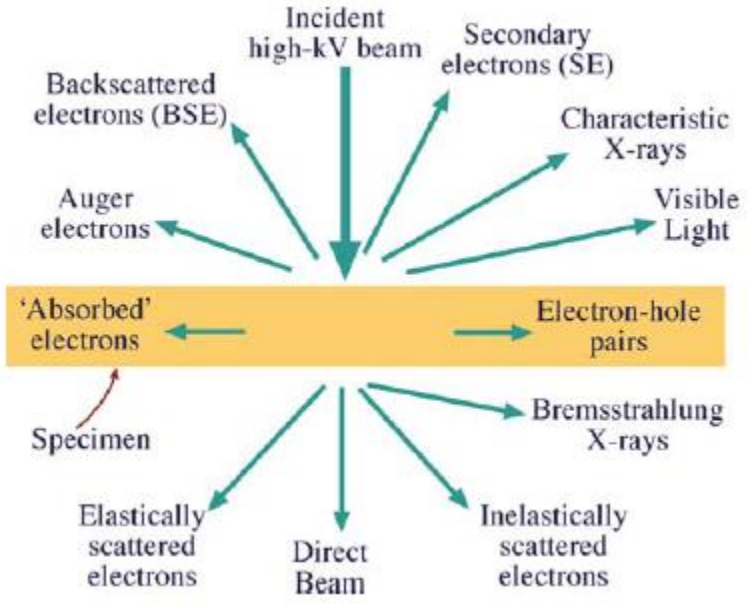

Figure 2.2 The signals generated by electron-specimen interaction (Williams & Carter, 2009).

2.3 Thermogravimetric analysis

Observation of the response of the materials when heated can be dated back to ancient times. However, the serious measurement is based on the invention of thermocouple at the end of 19th century. The development of thermal analysis applied to geosciences is from the experiment of La Chatelier in 1887 when he classified the different samples of clay by their dehydration point. In the1930s, it became a simple and inexpensive technology in the field of mineralogy, compared to X-ray diffraction (XRD) which was expensive during that time (Plante *et al.*, 2009).

Thermogravimetric analysis (TGA) is a common thermal analysis technique involving measuring the sample weight as a function of temperature or time while the sample is loaded on a precise thermobalance and subjected to a heating program in a controlled atmosphere (Prime *et al*., 2009). The components of the instrument are microbalance, furnace, programmer controller, and a computer (Fig. 2.3). The balance should be in a suitably enclosed system so that the nature and pressure of the atmosphere surrounding the sample can be controlled (Brown, 2001).

Thermogravimetric curves are plotted with the weight change on the vertical axis and temperature on the horizontal axis. However, this curve is difficult to interpret. Therefore, the first derivative of the weight loss curves (DTG) are plotted to assist in the interpretation and reveal the inflection points (Plante *et al.*, 2009).

Generally, TGA can provide information on physical and chemical properties. The physical properties include melting, evaporation, sublimation and adsorption while the chemical properties include dehydration, dissociation, oxidation and reduction. Specifically, TGA characterizes the decomposition and thermal stability of materials under various conditions including the specific temperature ranges and heating rates and to examine the kinetics of the physicochemical processes occurring in the sample (Sandler *et al*., 1998). For polymer nanocomposites, TGA is beneficial in quantifying the amount of the organic matter exchanged on the surface of the filler particles, thus generating an idea of the success or extent of the ion exchange process (Mittal, 2012). For clay minerals, the endothermic reactions occur with desorption of surface H_2O, dehydration of interlayer H_2O at low temperature ($<100^oC$), dehydroxylation at high temperature and melting. Exothermic reactions are related to recrystallization which are concurrent or after dehydroxylation and melting (Guggenheim & van Groos Koster, 2001).

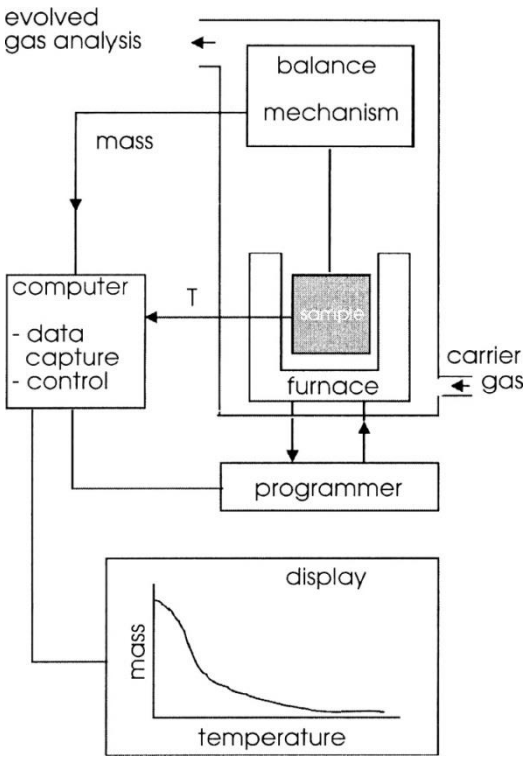

Figure 2.3 The scheme of TGA instrument (Brown, 2001).

2.4 Porosimetry

Porosity is the pore space inside the particle. There are two kinds of pores: open pores and closed pores. The open pore is the pore inside the particle but connected with the surface of the particle. The closed pore is totally inside the particle. According to size, the pores are divided into three categories: micropores (diameter <2nm), mesopores (diameter 2nm-50nm) and macropores (diameter >50nm) (Sing *et al*., 1985).

To measure the porosity, there are two methods: nitrogen adsorption and mercury porosimetry. The method we conducted in this experiment is nitrogen adsorption which can determine the several parameters of pore structure of the material such as pore volume, specific surface area and pore size. The range of pore diameters that the nitrogen adsorption can assess is from 0.3 to 300nm, which is not covered by mercury porosimetry measurement. During the desorption process, the isotherm is affected by the pore network. The hysteresis of the isotherm is due to the capillary condensation of the pores. Prior to the experiment of adsorption, in order to remove the physisorbed species from the surface of the adsorbent, the outgassing procedure is conducted which exposes the material to high vacuum and elevated temperatures. The condition of the outgassing such as the temperature programme, the change in pressure over the adsorbent and the residual pressure is controlled in order

to have a reproducible isotherm. Sometimes, it can be achieved by flushing the inert gas and heating instead of high vacuum (Sing *et al*., 1985; Sing, 2001).

The procedure of the experiment is to cool down the material to cryogenic temperature which is below -150^{o}C. Then, the adsorptive gas, which is normally is nitrogen, is inserted. At a constant temperature, the relationship between the quantity of nitrogen adsorbed and the pressure when the equilibrium is achieved is recorded. Afterwards, according to this result, the isotherm of adsorption and desorption is depicted. The isotherm of adsorption reveals the quantity of gas required to form the monolayer over the external surface of the material and from which to calculate the surface area (Sing *et al*., 1985).

The results shown in this experiment are mainly Type IV isotherms which are characteristic of micropores and some inherent inter-particle mesopores. However, the dominant feature of this isotherm is the hysteresis loop because the capillary condensation causing the adsorption and desorption isotherm are not matched (Yortsos, 1999).

Reference

Brown, M. E. (2001) *Introduction to thermal analysis: techniques and applications. Dordrecht* ; Norwell, Mass : Kluwer Academic Publishers.

Elsass, F. (2006). Transmission electron microscopy. In F. Bergaya, B. K. G. Theng & G. Lagaly (Eds.), *Handbook of Clay Science* (pp. 939-963). Amsterdam: Elsevier Science.

Guggenheim, S. & van Groos Koster, A.F. (2001). Baseline studies of the clay minerals society source clays: Thermal analysis. *Clays and Clay Minerals, 49*(5), 433-443.

Gunning, W.T. & Calomeni, E.P. (2000). A brief review of transmission electron microscopy and applications in pathology. *Journal of Histotechnology 23*(3) 237-246.

He, B.B. (2009) X-ray technology and its brief history. *Two-Dimensional X-ray Diffraction*. John Wiley & Sons.

Mark, L. & Rex, P. (2013). X-Rays and X-Ray Diffraction. *Structure Determination by X-ray Crystallography: Analysis by X-rays and Neutrons* (pp.111-159). Boston, MA: Springer US.

Mittal, V. (2012). Thermal Characterization of Fillers and Polymer Nanocomposites. *Characterization techniques for polymer nanocomposites*(pp.13-32). Weinheim :

Wiley-VCH.

Plante, A. F., Fernandez, J. M., & Leifeld, J. (2009). Application of thermal analysis techniques in soil science. *Geoderma, 153*(1-2), 1-10.

Prime, R. B., Bair, H. E., Vyazovkin, S., Gallagher, P. K. & Riga, A. (2009). Thermogravimetric analysis (TGA). In Menczel, J. D., Prime, R. B., Bair (Eds.) *Thermal analysis of polymers: fundamentals and applications*. Hoboken, NJ : John Wiley.

Reimer, L. & Kohl, H. (2008) *Transmission electron microscopy: physics of image formation.* New York, NY : Springer.

Sandler, S. R., Karo, W., Bonesteel, J. A. & Pearce, E. M. (1998). *Polymer synthesis and characterization: a laboratory manual* (pp.108-119). San Diego : Academic Press.

Sing, K. S. W., Everett, D. H., Haul, R. A. W., Moscou, L., Pierotti, R. A., Rouquérol, J. & Siemieniewska, T. (1985) Reporting physisorption data for gas/solid systems with special reference to the determination of surface area and porosity. *Pure and Appl. Chem. 57*, 603– 619.

Sing, K. (2001) The use of nitrogen adsorption for the characterisation of porous materials. *Colloids and Surfaces A*: *Physicochem. Eng. Aspects 187–188*, 3–9.

Williams, D. B. & Carter, C. B. (2009) *Transmission electron microscopy: a textbook*

for materials science. New York ; London : Springer.

Yortsos, Y. C. (1999). Probing Pore Structures by Sorption Isotherms and Mercury Porosimetry. In Wong, P. Z. (Eds.). *Methods in the physics of porous media* (pp. 69-117) San Diego : Academic Press.

Yoshio, W., Eiichiro, M. & Kozo, S. (2011) Diffraction from Polycrystalline Samples and Determination of Crystal Structure. *X-Ray diffraction crystallography: introduction, examples and solved problems* (pp.107-167). Berlin ; Heidelberg ; New York: Springer.

Chapter 3 : Physicochemical characterization of Portuguese clay

3.1 Introduction

A Portuguese clay from the North East city of Bragança (Fig. 3.1) was selected for this experiment. The geological information of the area where the sample was collected is mainly described by Pais (2012). According to the literature, the location of this sample belongs to Douro Basin (Fig. 3.2). The era of the formation is Cenozoic, in the transition series between Miocene to lower Pliocene. The category of this material is Castro Member of Bragança Formation (Pais, 2012). Therefore we named this sample as the abbreviation BRN.

The use of the clay minerals on the human body, especially in spas, is famous in Portugal as well as the scientific approach to the healing clays (Rebelo *et al*., 2010). There are two main types of applications for healing purposes, one is for external uses, such as in spas and topical applications, and another is for ingestion (Tateo & Summa, 2007). In this thesis, the properties of main concern were related to external use. According to Carretero *et al* (2006), the main properties of clay minerals used in spas and aesthetic medicine are:

1. Softness and small particle size to ease the discomfort when applied on the skin;
2. Rheological and plastic properties to form the viscous and consistent paste when adhered to the skin;

3. Similar pH with human body to avoid irritation;

4. High sorption capacity to absorb grease and toxins from skin and to incorporate with organic medicine for healing the human body;

5. High cation exchange capacity (CEC), enabling an exchange of nutrients (K^+ or Na^+) to take place while the clay mineral is in contact with the skin;

6. High heat-retention capacity to maintain the temperature when treating illnesses such as chronic rheumatic inflammations and dermatological problems.

The clay minerals used in spa centers are normally raw materials and a mixture of minerals. Besides phyllosilicates which are appropriate for healing purposes, the mixtures contain minerals such as Fe-Mn-(hydr)oxides, calcite, quartz and feldspars which should be controlled (Carretero *et al*., 2006; López-Galindo *et al*., 2007). The chemical inertness and low or null toxicity of the material also is a requirement for the topical application (Fakhfakh *et al*., 2005).

The determination of the mineralogical composition and quantity and defining different physicochemical and technical properties of the material BRN in order to see possibilities for use in topical applications was performed. The properties determined were: grain size distribution, mineralogical and chemical composition, pH, cation exchange capacity, swelling potential, abrasivity, Atterberg limit and cooling rate (temperature curve).

Figure 3.1 The schematic map of the city Bragança location (asterisk).

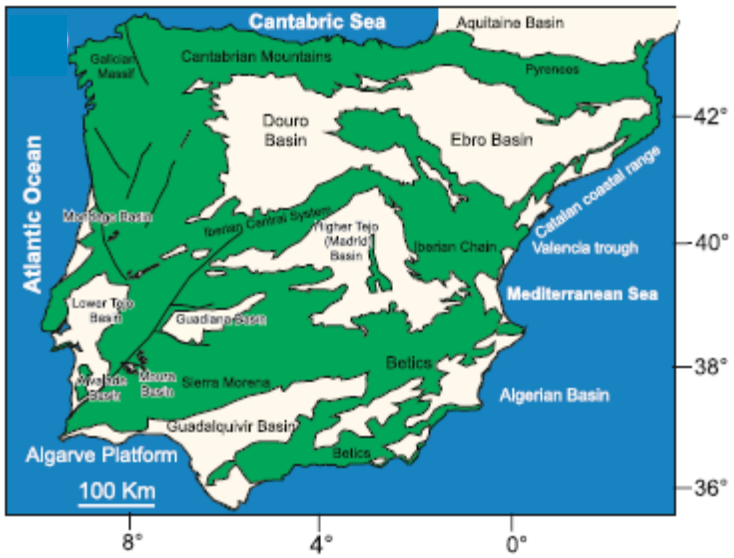

Figure 3.2 The schematic map of the main Iberia Cenozoic basin (Pais, 2012).

3.2 Experimental

1) Materials

This studied material BRN was collected from the North East city of Bragança in Portugal, and the coordinates are (41.805174, -6.790819). According to literature, the Bragança Formation sediments are immature and contain no hydrocarbon generation, but with moderately weathered feldspars in the sand fraction and a predominance of smectite and kaolinite in the clay fraction. The appearance of the sample is reddish in color (Fig. 3.3).

Figure 3.3 Photo of outcrop Bragança formation.

2) Methods

Grain separation & grain size distribution analysis

This study focuses on assessing the physicochemical properties of the silt-clay fraction (<63μm) of the sample, so the grain separation was conducted at the beginning. 500 grams of BRN raw sample was mixed with distilled water until it was well disintegrated and then wet-sieved by 63μm mesh. After that, the obtained two fractions were put into the oven to dry at 60^{o}C. The proportion of the two fractions was determined by their weight after drying. The <63μm fraction was then hand-ground by mortar and pestle and reserved for the following characterization. The precise analysis of the grain size distribution within silt-clay fraction was carried out by X-ray Sedigraph 5100 analyzer.

Mineralogical and chemical composition

The mineralogical composition of silt-clay fraction (<63μm) was carried out by a Phillips X-Pert diffractometer on random powder diffraction using Cu-Kα radiation with Ni-filter. For further assessment of the clay fraction (<2μm) composition, the sample was prepared by Stokes' law, deposited on a glass slide and air-dried for 24 hours at room temperature to form the oriented aggregates. The Oriented sample was

then further treated with ethylene-glycol and heated to 500^{o}C for comparing and determining the mineralogy of the clay fraction.

In order to have an idea about the quantity of every mineral in this sample, a semi-quantitative analysis was carried out by calculating the diagnostic peak areas of XRD patterns which were determined by full width at half maximum and peak height and weighing the empirically estimated factors or reflection powers. The content of each mineral (such as phyllosilicates and quartz) was decided by the silt-clay (<63µm) random powder XRD pattern. The quantity of each clay mineral (smectite, kaolinite and illite) was determined by the clay fraction (<2µm) oriented XRD pattern. Although this semi-quantitative analysis is not very precise and is only a rough estimate, the minerals' presence, absence, dominance and nondominance can be defined.

Chemical compositions of major, minor and trace elements were conducted by PANalytical Axios X-ray fluorescence spectrometer and flame photometer Corning 400. For the sample preparation, 10 grams of fine powder was mixed with 5 drops of poly(vinyl alcohol) forming a bit of an agglomeration and then the application of 15 tonnes for 20 seconds to make a pressed disk was performed. The unit expression of oxide-major element is in percentage and minor element is in ppm.

Physicochemical characterization

pH

For the pH measurement, 10 grams of sample were prepared by dispersion into 25mL distilled water for 1 hour with occasionally stirring. After calibration, the probe of the instrument HANNA pH meter HI9126 was immersed into the solution. The pH value and temperature were recorded at the same time.

Cation exchange capacity

Cation exchange capacity (CEC) was estimated by the ammonium acetate method. The sample was first saturated by ammonium acetate to exchange the interlayer cation by the ammonium ion. The remaining ammonium acetate was then washed away by ethanol 96%. The amount of ammonium ions in the interlayer was determined by re-exchanging them with magnesium ions and collection through distillation. The 0.1N hydrochloric acid was used to titrate the ammonium distillate with green bromocresol as indicator. The value of CEC was calculated as the equivalence of hydrochloric acid divided by the mass of sample.

Swelling potential

The swelling potential was carried out by Oedometer test according to the Portuguese norm NP 143-1965. The procedure was conducted as follows: the fine

grain sample was put into the metal ring to form the compacted cylindrical specimen, with the dried porous stone underneath and the probe of the pressure gauge above. The distilled water was then poured inside the device to the level of porous stone, so the specimen started to expand and change the point of the pressure gauge. The swelling change versus time, until the swelling nearly stops, was recorded and plotted as the swelling curve.

Abrasivity

The abrasivity was managed by the instrument Einlehner AT 1000. The procedure is to disperse 50 grams of fine grained sample into 500 mL distilled water by stirring well. There is a bronze wire on the bottom of the rotation stick of the instrument. The rotation stick was immersed into the solution and rotated. The bronze wire lost weight due to the friction with the material. The rotation speed was selected as 7250 rpm due to the hardness level of the material and then converted to basic value of 174,000 rpm in order to compare with other reference data. The abrasivity was calculated according to the weight loss before and after the experiment.

Atterberg limit

Atterberg limit of plastic index (PI) was determined by plastic limit (PL) and liquid limit (LL) according to the Portuguese norm NP 143-1969, where PI=LL-PL.

The plastic limit was measured by the rod method while the liquid limit was determined by the Casagrande method. Rod method was conducted by making the rod from material by adding adequate water. The plastic limit is defined as the water content in which the material-made rod crumbles at 3mm diameter while rolling. The Casagrande method was conducted by mixing water with material to make a paste and placed into the standard Casagrande cup. The paste was grooved and vibrated by the blows of the cup at a set frequency until the groove flowed and closed over a certain length. The number of the blows and the water content was noted and plotted as the curve. The liquid limit is defined as the water content corresponding to the 25 blows.

Cooling rate

The cooling rate measurement was presented by heating the 65 grams of dry material to 65^{o}C and then measuring the temperature by a Dual Channel Thermometer TM-906 A. The temperature changes were recorded every 30 seconds until the temperature decreased to 28^{o}C.

3.3 Results and discussion

Grain size distribution

The rough estimate of the proportion of sandy-gravel fraction (>63µm) and silt-clay fraction (<63µm) is 38.6% and 61.4% respectively. Grain size distribution analysis of the silt-clay fraction (<63µm) (Fig.3.4, Fig 3.5) showed that 47.4% mass contains particles that are <2µm which are the clay fraction, while the 52.6% fraction is the silt fraction and the mean equivalent spherical diameter is 2.26 µm. However, due to the aggregation phenomena, the real proportion of the clay fraction may exceed the estimated value. Those results of grain size distribution showed that this material is rich in fine grain particles and clay minerals which greatly affect the physicochemical properties such as the cation exchange capacity, cooling rate, plasticity, adhesiveness, swelling properties and abrasivity (Veniale *et al*., 2007). Meanwhile, the specific surface area and pleasant sensation when the material is applied on the human body are also related to the grain size (Veniale *et al*., 2007).

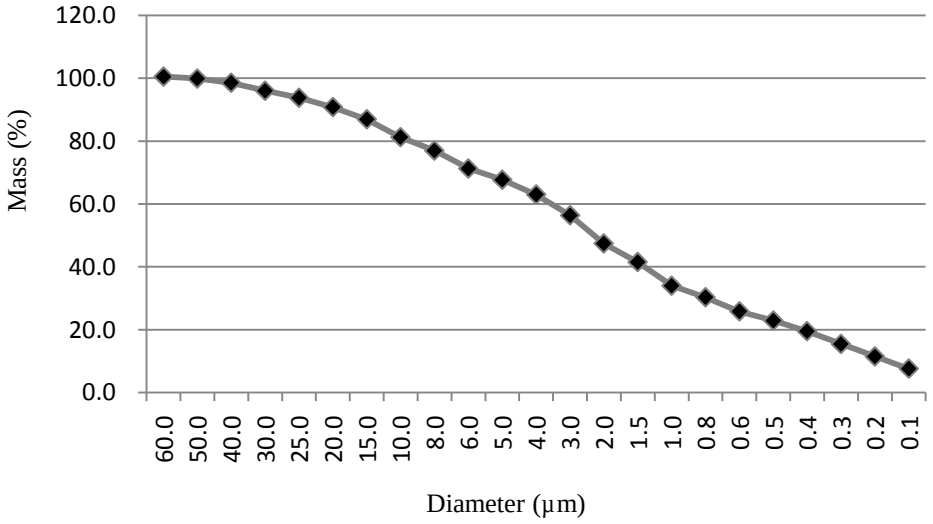

Figure 3.4 Cumulative mass percentage of silt-clay fraction.

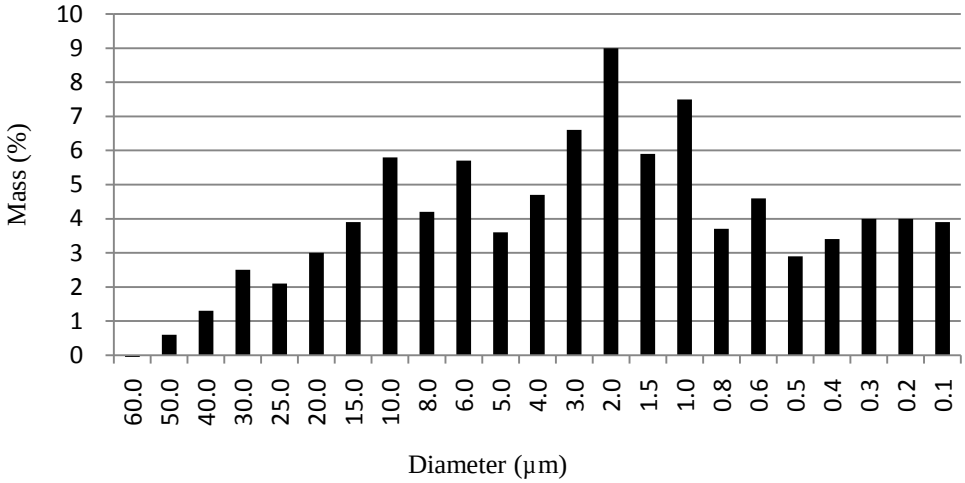

Figure 3.5 Mass population of silt-clay fraction.

Mineralogical and chemical composition

The mineralogical composition was determined by the semi-quantitative analysis of XRD patterns (Figure 3.6, 3.7, 3.8, 3.9 and Table 3.1a). The dominant mineral of this material is smectite at 47%. The other main components are illite at 23% and kaolinite at 17%. The overall clay mineral content estimated semi-quantitatively is 87%. However, the clay fraction (<2 μm) is 47.4% according to the grain size distribution result. The difference might be due to the coagulation of the clay mineral particles and they may not have been grounded well prior to the grain size distribution test. For other minerals, quartz and anatase, they are present at 5% and 4% respectively. Otherwise, there are still plagioclase, siderite, K-feldspar and hematite at1%. On the other hand, the chemical analysis (Table 3.1b) showed the main elements are SiO_2 55% and Al_2O_3 23% which correspond to phyllosilicate, quartz, K-feldspar and plagioclase. The Fe_2O_3 9% may refer to hematite and siderite while TiO_2 1% for anatase. As for the common exchangeable elements, potassium (K_2O) 2% and magnesium (MgO) 2% are greater than sodium (Na_2O) 0.1% and calcium (CaO) 0.2%. However, the main exchange cations should be examined, since only few of them attribute to cation exchange capacity (Rebelo, 2010). In addition, the content of potassium partially contributes to K-feldspar and the interlayer cation of illite. The loss on ignition value is 9%.

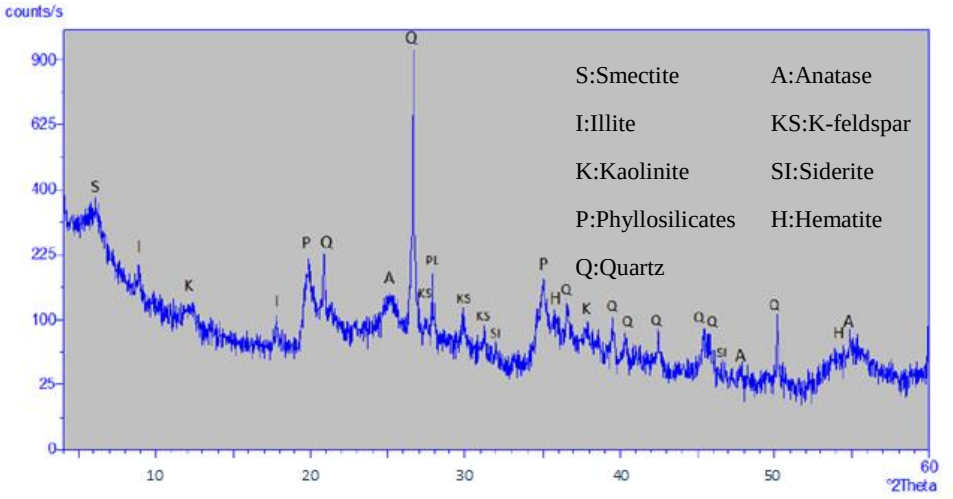

Figure 3.6 Powder XRD pattern of BRN (<63µm).

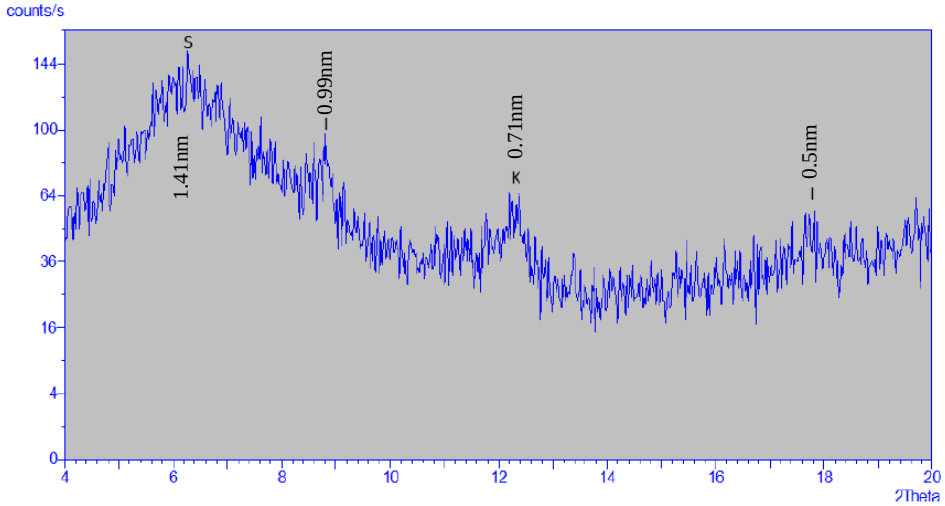

Figure 3.7 Oriented XRD pattern of BRN (<2 µm).

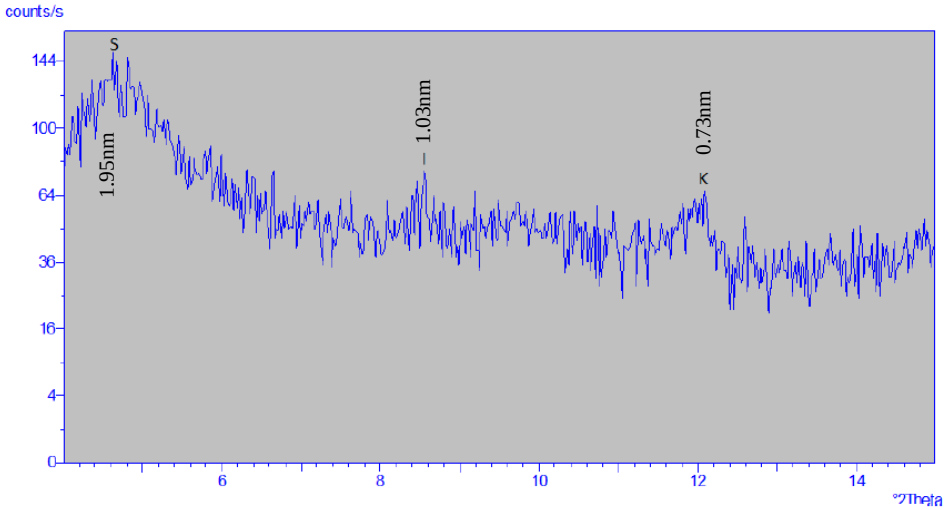

Figure 3.8 Oriented XRD pattern of BRN (<2 µm) - treated with ethylene-glycol.

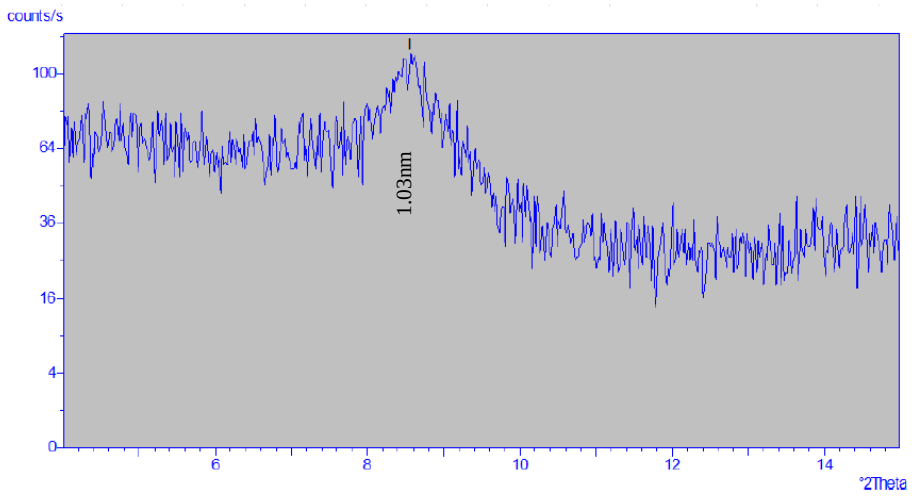

Figure 3.9 Oriented XRD pattern of BRN (<2 µm) – heated at 500°C.

(a)

Smectite	Illite	Kaolinite	Anatase	Quartz	Plagioclase	K-feldspar	Siderite	Hematite
47	23	17	4	5	1	1	1	1

(b)

Na_2O	MgO	Al_2O_3	SiO_2	P_2O_5	SO_3	K_2O	CaO	TiO_2	Fe_2O_3	LOI
0.1	2	23	55	0.1	0.02	2	0.2	1	9	9

Table 3.1 Mineralogical and chemical composition. (a) Mineralogical composition (wt.%) (b) Major elements (wt.%). *LOI: loss on ignition.

The Table 3.2 shows the content of elements detected in the material and comparison with the standard limit of hazardous elements. The limits are according to the "Permitted Daily Exposure" (PDE) which defines on a chronic basis, the pharmaceutically maximum acceptable exposure to an element which does not produce any adverse health effects (Health Canada, 2009; EMEA, 2008; USP, 2010; Rebelo *et al*., 2011a). Class 1 hazardous elements are defined as toxic to humans, environmentally hazardous, and should be essentially absent. Sb is included in class 1 elements through the ministry of health in Canada (Health Canada, 2009). The elements in class 2 have less toxicity than those in class 1 but should be limited in pharmaceuticals. In this studied sample, the amounts of As and Pb are over the limit. However, the bio-availability test of both elements should be done to know the exact amount adsorbed by body in the conditions of dermal and oral applications. According to the reference, in terms of dermal application, As absorbed from the skin is less than 1% of the absorption through ingestion. Otherwise, the content of Pb is relatively low compared to other sediments which usually contain 30 to 300ppm (Rebelo *et al*., 2011a). Cd is detected in this sample, but still in an acceptable amount. Moreover, concerning the hazardous elements in class 2, all of them are within the PDE concentration. Regarding topical applications, bio-availability tests should be conducted to analyze the release rate of trace elements between skin and material in

varied conditions and the relationship between elements and minerals (Tateo & Summa, 2007). Those results are more practical in the real situation than the concentration value. In addition, it should be noted that the material is in a salty environment which simulates the condition of body sweat. According to leaching test done by Summa & Tateo (1998), the leaching rate of elements in salty solution is greater than in pure water.

hazardous elements	detected amount	component limit	other elements	detected amount	other elements	detected amount
class 1			Zn	124	Se	1
As	28	15	Ga	26	Br	5
Cd	5	5	Sc	21	Rb	105
Pb	22	10	Sr	52	U	3
Sb	nd	5	Y	48	Ba	395
			Zr	114	Ge	nd
class 2			Nb	13	Ag	nd
Cr	176	250	Co	37	Sb	nd
Cu	63	2500	Sn	4	Te	nd
Mn	526	2500	Ti	3	I	nd
Mo	1	250	La	34	Yb	nd
Ni	124	250	Th	9	Hf	nd
V	145	250	Ce	79	Ta	nd
			Nd	40	W	nd
			Sm	9	Bi	nd
			Cs	9		

Table 3.2 Trace elements and the limit standard of the hazardous elements (ppm). (nd means not detected).

Physicochemical characterization

pH

In this sample, the pH value measured at 25.6 ^{o}C is 4.72 which is more acidic than the human body (pH 4-6.5). Further pH measurements of the mud form of the material should be conducted to simulate the real conditions of topical application because the pH value can influence consistency and activity of clays (Veniale *et al*., 2007) and also affects the bio-availability of both desired and hazardous elements (Tateo & Summa, 2007).

Cation exchange capacity

The value of cation exchange capacity (CEC) is 20.7 cmol/kg and this is mainly attributed to the content of smectite and illite (Rebelo *et al*., 2010). The siderite content, which presents a small amount of carbonate, affects the CEC result. During the experiment, the carbonate is partially dissolved and interacts with the electrolyte-rich solution (Dohrmann, 2006).

Swelling potential

The value of the swelling potential (Fig 3.10) is 36.19% which is related to the compensation between the proportion of swelling clay smectite and other non-swelling minerals.

Abrasivity

The value of abrasivity is related to the pleasant sensation of topical application and is mainly affected by the grain size and hard minerals (quartz, plagioclase, K-feldspar and hematite). According to the research by Klinkenberg *et al*. (2009), with smaller particle sizes, there is a higher abrasivity due to more sharp edges caused by breaking the hard minerals. In this material, at 174,000 rpm, the abrasivity value 196 g/m^2 is softer, compared to the acceptable value for the topical application which is 870 g/m^2 (Gomes, 2002 cited by Rebelo *et al*., 2011b), but harder than bentonite 84 g/m^2 (Klinkenberg *et al*., 2009).

Atterberg limit

For the Atterberg limit, the value of the plastic index is 13% which is obtained by subtraction of the liquid limit 39% and plastic limit 26%. According to Bain (1971) and cited by Rebelo *et al*. (2011b), the material with liquid limit below 50% is the low plasticity clay. The Jenkins soils classification (Gomes, 2002) indicates the sample with the plastic index > 15% is the high plasticity soil while in this sample the value is close and less plastic. With a good plastic behavior, the water retention capacity is increased and the material is adequate in manipulating and spreading for topical

applications. The higher water limit is followed by higher plastic limit (Rebelo *et al*., 2011b).

Cooling rate

The cooling rate depends on many characteristics such as the texture, composition, specific heat, and heat diffusiveness of the clay (Fakhfakh *et al*., 2005). The result of a cooling rate (Fig. 3.11) from 65^{o}C to 28^{o}C lasting 59 minutes is enough for topical applications which usually take 15-30 minutes (Rebelo *et al*., 2010). This is compromised by the content of smectite which slows the cooling rate and improves the thermal therapeutic properties (Legido *et al*., 2007). Moreover, the Fe-content of minerals siderite and hematite in this sample are also favorable for the low heat release (Venial *et al*., 2007). A further cooling rate test in mud conditions should be done in order to simulate the conditions of topical application, and is expected to be slower because of the heat capacity of water (Ferrand & Yvon, 1991).

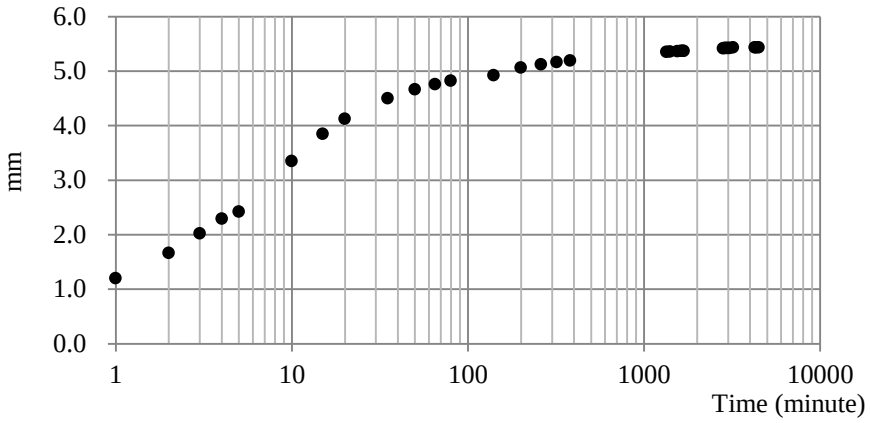

Figure 3.10 Swelling curve.

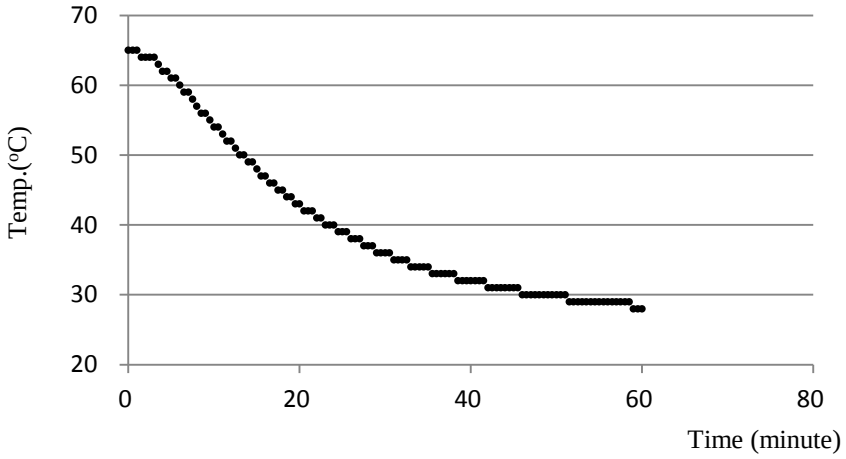

Figure 3.11 Cooling rate curve.

Conclusion

In this studied material BRN, the particle size <2µm representing the clay fraction which is the rich fine grained sample among the silt-clay fraction (< 63µm) is 47.4%. The silt-clay fraction (< 63µm) has a high content (87%) of clay minerals where smectite is 47%, illite is 23% and kaolinite is 17% according to the semi-quantitative analysis. The properties of this sample are mainly influenced by smectite and less affected by illite and kaolinite. The chemical composition corresponds to the components of minerals. The possible exchangeable cations are Mg^{2+} and K^{+}; a further test should be done for the confirmation. The material contains the class 1 hazardous elements As, Pb and Cd in quantities not allowed in oral applications, but might be acceptable for topical applications. For the physicochemical characterization for healing purposes, the pH of this material is weakly acidic. The cation exchange capacity and swelling potential are in medium range and are related to the smectite content. The mild abrasivity attributed by the small amount of minerals quartz, plagioclase, K-feldspar and hematite is allowed for topical applications. The plastic index is in the medium range while the cooling time is long enough to apply for topical use. Generally, the attention should be paid to the hazardous elements when used for topical and oral applications. In order to examine

the relationship between elements, minerals and the human body, further bio-availability tests should be conducted.

Reference

Bain, J.A. (1971). A plasticity chart as an aid to the identification and assessment of industrial clays. *Clay Minerals 9*, 1–17.

Carretero, M. I., Gomes, C. S. F. & Tateo, F. (2006). Clays and human health. In F. Bergaya, B. K. G. Theng & G. Lagaly (Eds.), *Handbook of Clay Science* (pp. 939-963). Amsterdam: Elsevier Science.

Dohrmann, R. (2006). Cation exchange capacity methodology I: An efficient model for the detection of incorrect cation exchange capacity and exchangeable cation results. *Applied Clay Science, 34* (1-4), 31-37.

EMEA (2008). Guideline on the Specification Limits for Residual Metal Catalysts for Metal Reagents Available at: http://www.ema.europa.eu/docs/en_GB/document_library/Scientific_guideline/2009/09/WC500003586.pdf

Fakhfakh, E., Chakroun, I., Chaari, I., Medhioub, M., Rocha, F., Gomes, C., Lopez-Galindo, A., Kooli, F., Zargouni, F. & Jamoussi, F. (2005) Chemical and physical characterization of some Tunisian smectites for human healing use. *ActaGeodyn. Geomater .2*(138), 39-45.

Ferrand, T. & Yvon, J. (1991). Thermal properties of clay pastes for pelotherapy. *Applied Clay Science, 6*, 21-38.

Gomes, C. (2002). Argilas. Aplicações na Indústria, O Liberal Câmara de Lobos,

Madeira.

Health, Canada (2009). Draft Guidance on Heavy Metal Impurities and Cosmetics. Available at: http://www.hc-sc.gc.ca/cps-spc/pubs/indust/heavy_metals-metaux _lourds/index-eng.php

Klinkenberg, M., Kaufhold, S., Dohrmann, R. & Siegesmund, S. (2009). Abrasivity of bentonite dispersions. *Applied Clay Science,46,* 37–42.

Legido, J.L.,Medina, C., Mourelle, M.L., Carretero, M.I. & Pozo, M. (2007). Comparative study of the cooling rates of bentonite, sepiolite and common clays for their use in pelotherapy. *Applied Clay Science, 36,* 148-160.

Lopez-Galindo, A., Viseras, C. & Cerezo, P. (2007). Compositional, technical and safety specifications of clays to be used as pharmaceutical and cosmetic products. *Applied Clay Science, 36*(1-3), 51-63.

Pais, J. (2012) *The Paleogene and Neogene of Western Iberia (Portugal): a Cenozoic record in the European Atlantic domain* (pp.1-24). Heidelberg ; New York : Springer.

Rebelo, M., Rocha, F. & Da Silva, E. F. (2010). Mineralogical and Pysicochemical characterization of selected Portuguese Mesozoic-Cenozoic muddy/clayey raw materials to be potentially used as healing clays. *Clay Minerals,45*(2), 229–240.

Rebelo, M., Viseras, C., López-Galindo, A., Rocha, F. & da Silva, E.F. (2011a). Characterization of Portuguese geological materials to be used in medical hydrology. *Applied Clay Science,51*(3), 258-266.

Rebelo, M., Viseras, C., López-Galindo, A., Rocha, F. & da Silva, E.F. (2011b). Rheological and thermal characterization of peloids made of selected Portuguese geological materials. *Applied Clay Science, 52* (3), 219-227.

Summa, V. & Tateo, F. (1998). The use of pelitic raw materials in thermal centres: Mineralogy, geochemistry, grain size and leaching tests. Examples from the Lucania area (southern Italy). *Applied Clay Science, 12* (5), 403-417.

Tateo, F. & Summa, V. (2007) Element mobility in clays for healing use. *Applied Clay Science 36* (1-3), 64–76.

USP, The United States Pharmacopeial Convention (2010). <232> Elemental Impurities—Limits. Pharmacopeial Forum, 36(1). Available at: http://www. usp.org/sites/default/files/usp_pdf/EN/USPNF/key-issues/232Elemental Impurities.pdf

Veniale, F., Bettero, A., Jobstraibizer, P. G. & Setti, M. (2007).Thermal muds: Perspectives of innovations. *Applied Clay Science, 36*, 141–147.

Chapter 4 : Nanocomposites with Polylactide

4.1 Introduction

Since the 1990s, plastic has played an important role in human daily life especially for packaging which is the main purpose for plastic use. However, most of the plastics are made from fossil fuels and are not degradable, thus creating a huge waste impact on the environment. Therefore, except for building the landfill site to bury those wastes which also causes other problems, an alternative is to develop the biodegradable polymers (Ray & Bousmina, 2005).

Biodegradable polymers can be made from biosources such as corn, wood cellulose or derived from petroleum. However, the biodegradable polymers from renewable sources such as polylactide are attracting more attention since the origin is eco-friendly (Ray & Bousmina, 2005).

However, the properties of biodegradable polymers cannot compete with the conventional petroleum-based polymers. Therefore, the reinforcing of biodegradable polymers with inorganic fillers was developed to make composites and increase properties such as thermal stability, gas barrier properties, strength, low melt viscosity, and slow biodegradation rate. After, the development of composites advanced to the nanoscale, this resulted in creating high aspect ratios and high specific surface areas with addition of a low amount of nanofiller (≤5wt.%), which can match the efficiency

of conventional composites with a higher amount of filler (40-50%) (Ray & Bousmina, 2005).

There are various nanoreinforcements being developed such as nanoclays (layered silicates), cellulose nanowhiskers, ultra-fine layered titanate and carbon nanotubes. Among them, organically modified layered silicates have the advantages of being inexpensive and easily available (Ray & Bousmina, 2005).

There are two types of polymer/ layered silicate nanocomposites according to the strength of interaction. One is the intercalated nanocomposite, where the insertion of polymer chains into the silicate structure occurs with crystallographic regularity. Another is exfoliated nanocomposites, in which the individual silicate layers are separated in a polymer matrix randomly (Fig 4.1) (Ray & Bousmina, 2005).

The method to prepare polymer/layered silicates is to intercalate polymers into the silicate galleries generally by two ways: 1. insertion of suitable monomers in the silicate galleries and subsequent polymerization and 2. direct insertion of polymer chains into the silicate galleries from either solution casting or the melt blending (Ray & Bousmina, 2005).

In previous research on a polylactide/ layered silicate nanocomposite, Ogata *et al* (1997) used the solution casting method and ended up with a micrometer-phase separation but without nanometer-range dispersion of silicate layers. Afterwards, Ray

et al. (2002) and Maiti *et al*. (2002) were able to produce the intercalated polylactide/ layered silicate nanocomposite by organically modified clay and melt intercalation. Research both by Krikorian & Pochan (2003) and Pluta (2006) showed success in using the melt blending method to produce the exfoliated polylactide/ layered silicate nanocomposites. The work done by Wu, T. -M. & Wu, C. -Y. (2006) revealed a successful solution casting method to make the exfoliated nanocomposite by adding chitosan to improve the chemical similarity between the PLA and the organically modified montmorillonite.

Montmorillonite belongs to the smectite group, which are 2:1 layer clay minerals. The hydrous cations inside the interlayer space make it a swelling clay with the ability to exchange cations. However, the ability of pristine montmorillonite to be intercalated by polymers is limited because of the hydrophilic property of the interlayer. In order to change the property from hydrophilic to organophilic, the interlayer should be treated by organic compounds which become the organophilic medium; the most frequently used ones are the quaternary alkylammonium ions such as cetyltrimethylammonium bromide (CTAB) (de Paiva *et al*., 2008).

In this part of the experiment, intercalation of the Portuguese raw material (BRN) with polylactide by the solution casting method was attempted, and characterization was performed by x-ray diffraction (XRD) and transmission electron microscopy

(TEM). Moreover, since the BRN sample mainly contains smectite, the pure montmorillonite was also prepared with polylactide to make a nanocomposite using the same procedure, in order to compare the differences. Thermogravimetric analysis (TGA), infrared analysis (IR), nitrogen adsorption porosimetry and nuclear magnetic resonance (NMR) were conducted to measure the different properties between them.

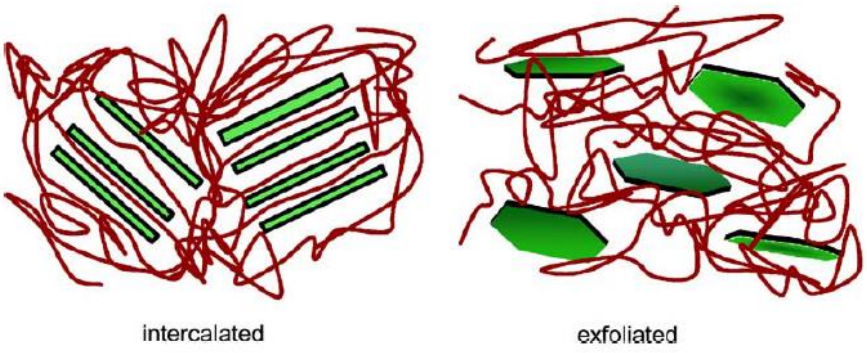

Figure 4.1 The scheme of two different types of polymer/ layered silicate nanocomposites (Ray & Bousmina, 2005).

4.2 Experimental

1) Materials

Poly(D,L-lactide) (mol wt 75,000-120,000) (PLA) and cetyltrimethylammonium bromide (CTAB) were purchased from Sigma-Aldrich and used directly. The CTAB structure is shown as Figure 4.2. PLA was stored in the desiccator preventing hydrolysis. Wyoming montmorillonite SWy-2 (MMT) was obtained from the Clay Minerals Society located at Purdue University, West Lafayette, Indiana, USA. The raw montmorillonite was purified by the following procedure: 1. Size fractionation by sedimentation according to Stoke's law to eliminate impurity minerals such as quartz. 2. The formation of Na-MMT by Na^+ exchange process was done by adding MMT inside 1M NaCl solution. 3. In order to remove excess salt, the Na-MMT was washed with water and recuperated by centrifugation and this was conducted 4 times. Lastly, the Na-MMT was dialyzed with deionized water for 1 week (Carrado *et al*., 2006). Portuguese clay (BRN) was sedimented in order to collect the clay fraction (<2μm).

Figure 4.2 The structure of cetyltrimethylammonium bromide (CTAB).

2) Nanocomposite preparation

Through the analysis of the mineralogical composition of BRN sample, it was found that smectite was dominant within the clay fraction (<2μm). Therefore, preparation of MMT/PLA nanocomposite was also performed, in order to compare it with that of BRN/PLA. The nanocomposite synthesis was prepared by the solution-casting method. The procedures for both nanocomposites' preparation are as follows:

1. The clay fraction (<2μm) of sample 2g was dispersed into 250 mL of distilled water with stirring for 2 hours. Then, the clay modification with CTAB was carried out by adding the equivalent of 2 CEC amount of CTAB into the clay solution with vigorous stirring for several days until the interlayer space expansion was maximized, which was checked by XRD. After that, the solution was washed by ethanol using filtration to remove excess CTAB and checked by XRD. The wet clay was dried in the oven at 60^{o}C over night and then hand-ground into a powder. Those samples are named m-MMT and m-BRN as the organically modified montmorillonite and BRN. The blank MMT without modification by CTAB was prepared.

2. Different concentrations of 3%, 5% and 8% of MMT, m-MMT and m-BRN were respectively applied to polylactide. Each mixture was prepared around 100mg and the addition of 7mL of chloroform as the solvent. The solution was magnetically

stirred until the clay was dispersed. Ultrasonic stirring was applied for 30 minutes to the solution followed by stirring magnetically for 1 day. Lastly, the solution was dried in the vacuum oven at 60^{o}C for 1 day to produce films of dried clay/PLA. The proportion of each prepared complex is listed in Table 4.1.

Complex	Proportion
MMT3%/PLA:	3% unmodified MMT with 97% PLA
MMT5%/PLA:	5% unmodified MMT with 95% PLA
MMT8%/PLA:	8% unmodified MMT with 92% PLA
m-MMT3%/PLA:	3% modified MMT with 97% PLA
m-MMT5%/PLA:	5% modified MMT with 95% PLA
m-MMT8%/PLA:	8% modified MMT with 92% PLA
m-BRN3%/PLA:	3% modified BRN with 97% PLA
m-BRN5%/PLA:	5% modified BRN with 95% PLA
m-BRN8%/PLA:	8% modified BRN with 92% PLA

Table 4.1 The proportion of each complex.

3) Characterization

The XRD analysis was carried out by Philips PW 3710 diffractometer with Ni-filtered Cu Kα radiation (λ =1.54050 Å). Thermogravimetric analysis (TGA) was performed utilizing SDT 2960 instrument under N_2 flow (120 mL/min) with a heating rate of 10℃/min from room temperature until 1100^{o}C. Nitrogen adsorption porosimetry was conducted by Micromeritics ASAP-2010 instrument, with N_2 used as an adsorbent at 77K. TEM analysis was performed by a JEOL JEM-2100F TEM. For preparation, samples were embedded in an epoxy resin (Araldite 502, dodecenyl succinic anhydride (DDSA), DMP 30), cured at 60 ℃ overnight, and subsequently microtomed at room temperature into ultrathin slices (<100 nm thickness). IR spectra were recorded by Thermo Nicolet Nexus 670 FTIR under dry air. The preparation of KBr pellets and the attenuated total reflectance (ATR) were conducted. The ATR is the method to measure the sample as the powder state instead of the pellet form. The sample was cleaned from the apparatus by isopropanol between each measurement to ensure the accuracy. The ^{13}C NMR CP/MAS solid state spectra were collected using Bruker Avance III 200 NMR spectrometer.

4.3 Results and discussion

X-ray diffraction (XRD)

The XRD patterns of MMT and m-MMT (Fig. 4.3) show the 001 reflection of MMT shifted from high diffraction angle to low diffraction angle after the clay was modified by cetyltrimethylammonium bromide (CTAB), indicating an expansion in the basal spacing from 1.14 nm to 1.78 nm according to Bragg's law. The measurement of the interlayer spacing is made by subtracting the thickness of the silicate layer (0.95 nm) from the basal spacing (Ruiz-Hitzky *et al.*, 2005). The arrangement of the intercalated surfactant cations depends on the layer charge and the alkyl chain length (Lagaly, *et al.*, 2006). Alkylammonium ions in the interlayer space of smectites are typically arranged as monolayers (d_{001}~1.4 nm), bilayers (d_{001}~1.8 nm), pseudotrimolecular (d_{001}~2.2 nm) or paraffin-type (d_{001}>2.20 nm) (Hrachova *et al.*, 2010). Monolayers are arranged with short chain alkylammonium ions, while bilayers are arranged with longer chain ions and both chains are parallel to the silicate layers. The monolayer rearranges into the bilayer when the area of the flat-lying alkylammonium ions becomes larger than the equivalent area. A paraffin-type involves an orientation where the alkyl chains are standing with tilting angles (Lagaly, *et al.*, 2006). The 001 reflection for m-MMT is 1.78 nm which is in agreement with bilayer arrangement. The 002 and 003 reflections of m-MMT are observable in the

pattern which shows a good crystallization.

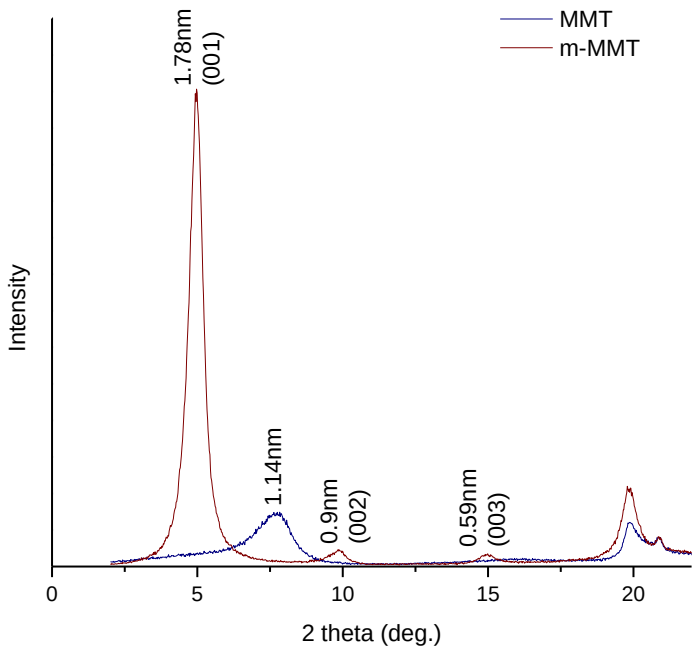

Figure 4.3 XRD patterns of MMT and m-MMT (<2μm).

Compared to MMT and m-MMT, the XRD patterns of BRN and m-BRN shown in Figure 4.4 (<63μm) and Figure 4.5(<2μm) reveal the extra peaks of illite and kaolinite. The reflection peaks of illite and kaolinite were unchanged after BRN modification by CTAB and this reveals that those minerals are not affected by the modification which is consistent with their properties. On the other hand, the reflection peak of smectite is shifted from 1.35nm to 2.4nm in the silt-clay fraction (<63μm), which is the paraffin-type, and to 1.85nm in the clay fraction (<2μm), which corresponds to an interstratification of the bilayer and pseudotrimolecular layer complexes due to the varying layer charge of layers (Ogawa *et al.*, 1995; Ramirez *et al.*, 2005).

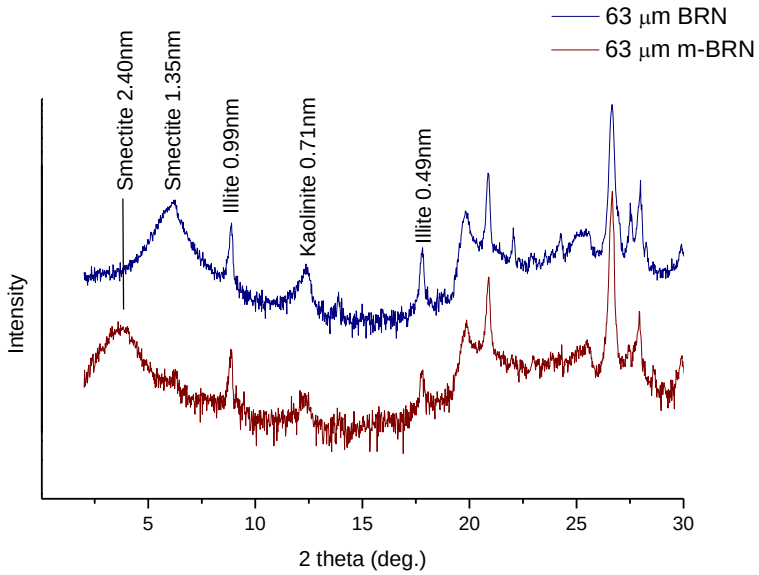

Figure 4.4 XRD patterns of BRN and m-BRN (<63μm).

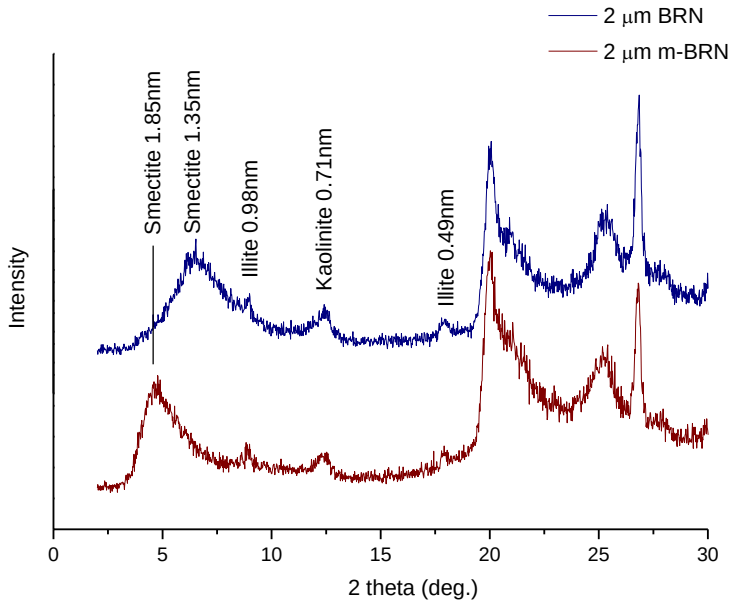

Figure 4.5 XRD patterns of BRN and m-BRN (<2μm).

The XRD pattern of polylactide is shown as Figure 4.6 and the polylactide complex with different concentrations of MMT and m-MMT are presented in Figures 4.7 and 4.8. Figure 4.7 showed that with a greater concentration of MMT, MMT/PLA has a more intense 001 reflection peak of MMT but a weaker reflection peak of PLA. Compared to Figure 4.3, the basal spacing of MMT/PLA shifted from 1.14nm to 1.37nm, indicating that the intercalated PLA has a monolayer arrangement. On the other hand, Figure 4.8 showed m-MMT3% and 5% PLA complexes have no peaks indicating the presence of interlayer distances at least larger than 4.8nm or no regular periodicity due to exfoliation (Wu, T. -M. & Wu, C. -Y., 2006). However, this result needs to be confirmed by TEM. The m-MMT 8%/PLA has a broadened peak for the 001 reflection, which might be due to the partial disruption of the clay stacking because of the high amount of nanofiller (Krikorian & Pochan, 2003).

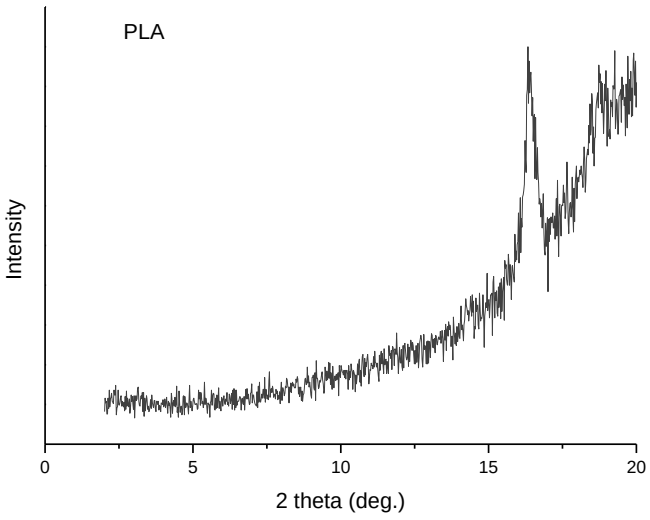

Figure 4.6 XRD pattern of PLA.

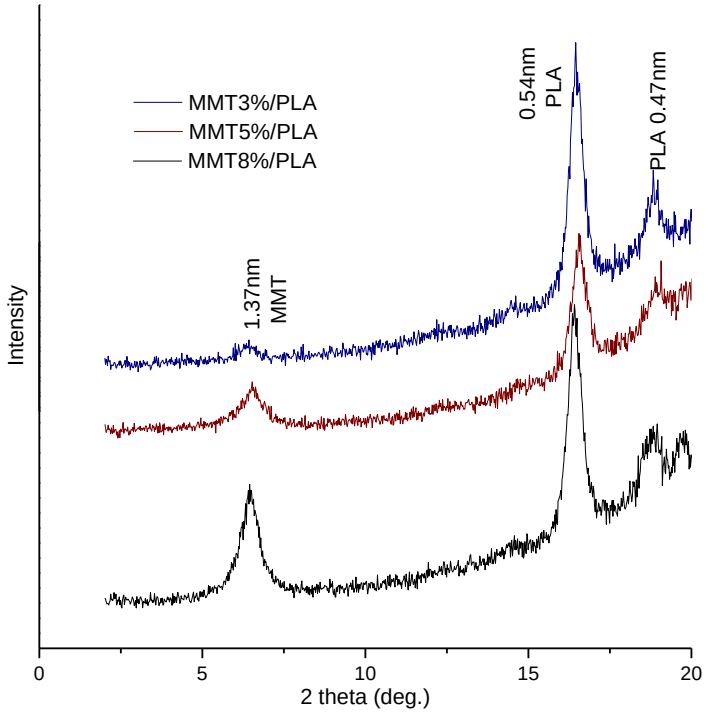

Figure 4.7 XRD patterns of MMT/PLA with different concentration (3%, 5%, 8%).

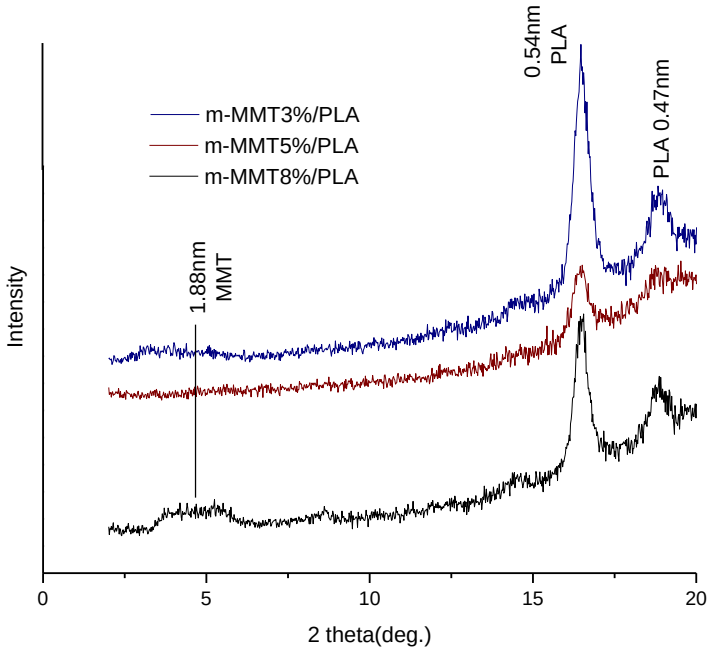

Figure 4.8 XRD patterns of m-MMT/PLA with different concentration (3%, 5%, 8%).

The XRD patterns of m-BRN/PLA were presented in Figure 4.9. Those XRD patterns show that the reflection peaks of illite and kaolinite are still present after mixture, but the reflection peak of smectite disappears in the case of three different concentrations of PLA. Similar to the case of montmorillonite, this result might be caused by exfoliation but the confirmation by TEM is needed.

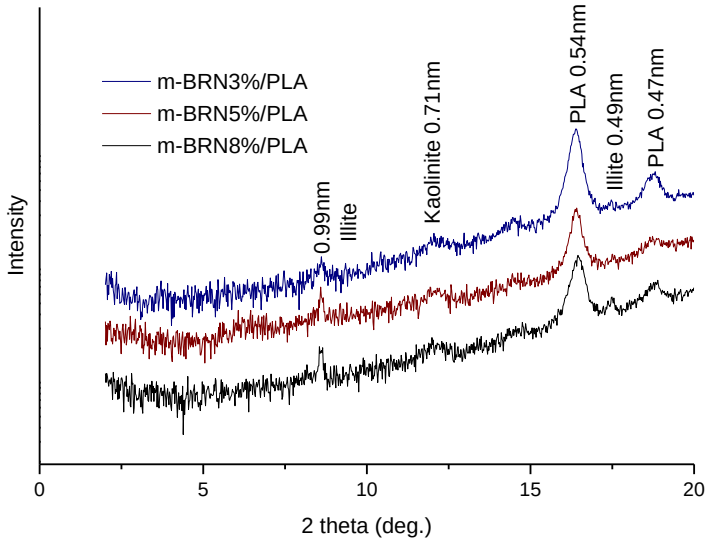

Figure 4.9 XRD patterns of m-BRN /PLA with different concentration (3%, 5%, 8%).

Transmission electron microscopy (TEM)

In order to assess the degree of the dispersion, m-MMT8%/PLA which has the broadened reflection peak, was imaged by TEM. The result is shown in Figure 4.10. The gray lines are the silicate layers inside the PLA matrix (bright area). There are clay platelets (point A) with interlayer spacing around 2.25nm and stacks (point B) within the sample. The stacks explain the decreased intensity of 001 reflection peak of the XRD pattern (Tenn et al., 2013; Martín *et al.*, 2009).

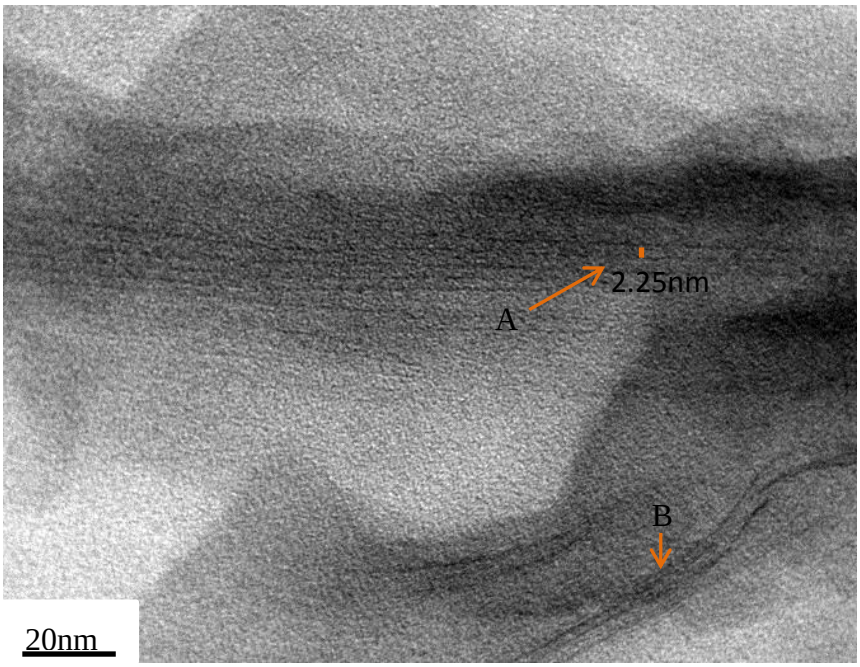

Figure 4.10 The TEM micrograph of m-MMT8%/PLA.

Thermogravimetric analysis (TGA)

The results of TGA are discussed in relation to the thermal ability and recognition of the components of the blends. In Figure 4.11, the TG curve shows the total weight loss of m-MMT as 25% and MMT as 10%. Figure 4.12 DTG curve shows that MMT and m-MMT have endothermic signals between 25 ^{o}C -100 ^{o}C and 500 ^{o}C-700 ^{o}C, representing the loss of surface water and structural water (bonded OH that undergoes dehydroxylation) respectively. The range for the release of water is broad and occurs in a two –step process (25 ^{o}C -100 ^{o}C) with the third peak centered at 360 ^{o}C, indicating the different environments of water existing in montmorillonite. Weakly bound, physisorbed water and free water pockets located within the aggregate structure evaporate within the lower temperature range. The interlayer water, along with water of the hydration sphere of the interlayer sodium cations, evaporates within the higher temperature range (Hoidy *et al.*, 2009; Xie *et al.*, 2001). Moreover, m-MMT has two extra absorption peaks centered at 313 ^{o}C and 424^{o}C representing the loss of alkylammonium ions from the interlayer. The decompositions occurring within two temperature ranges represent different bonding between alkylammonium ions and the clay layer. The alkylammonium lost at low temperatures has van der Waals interactions with other ions and is located on the exterior of the clay layer, while the alkylammonium lost at high temperatures interacts electrostatically with the

clay surface (Xi *et al*., 2005).

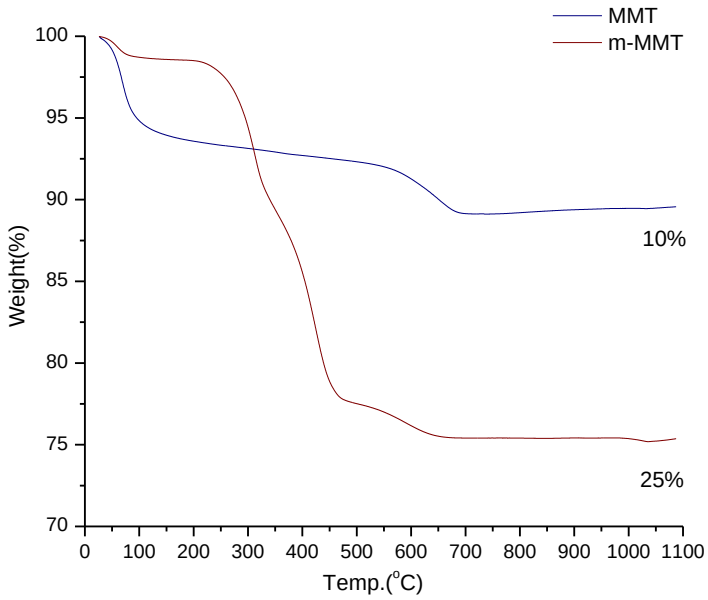

Figure 4.11 TG curves of MMT and m-MMT (<2µm).

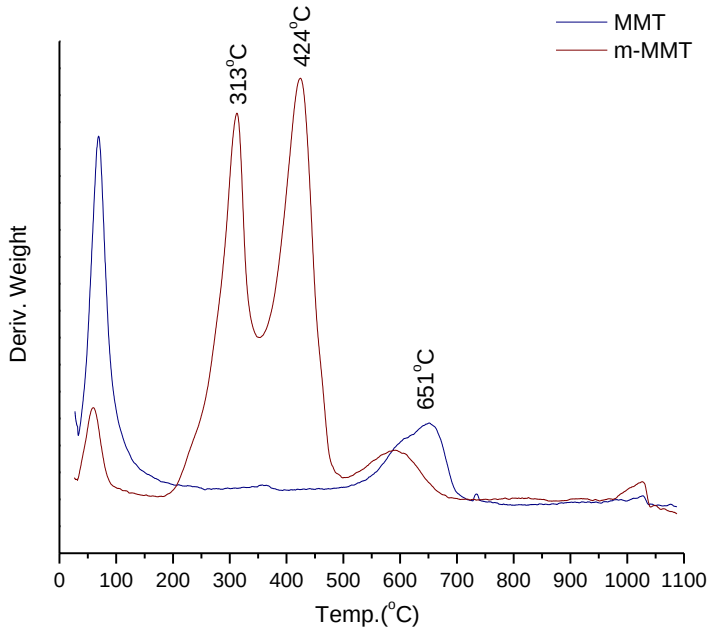

Figure 4.12 DTG curves of MMT and m-MMT (<2µm).

In the case of BRN and m-BRN, Figure 4.13 showed the total weight loss of BRN as 15% and m-BRN as 23%. Compared to the 10% weight loss of MMT and 15% weight loss of BRN, the difference between them might be due to more organic matter inside the BRN. Moreover, the CTAB modified clay has a greater weight loss than unmodified clay because of the loss of alkylammonium ions; this supports the result that the clay was successfully modified by CTAB (Hoidy *et al.*, 2009; Xie *et al.*, 2001).

Figure 4.14 shows the DTG results of BRN and m-BRN which have peaks centered at 100 ^{o}C and 475 ^{o}C, representing the release of surface water and structural water (dehydroxylation). The peak centered at 475 ^{o}C for m-BRN is not observed due to overlap by the peak centered at 415 ^{o}C. The difference in the dehydroxylation temperatures between MMT (651 ^{o}C) and BRN (475 ^{o}C), might be due to the 9% iron content of the BRN, since there is lower temperature required for dehydroxylation of iron hydroxides compared to aluminum hydroxides (Letaïef *et al*., 2003). In m-BRN, the temperatures of decomposition of alkylammonium ions are centered at 280 ^{o}C and 415 ^{o}C.

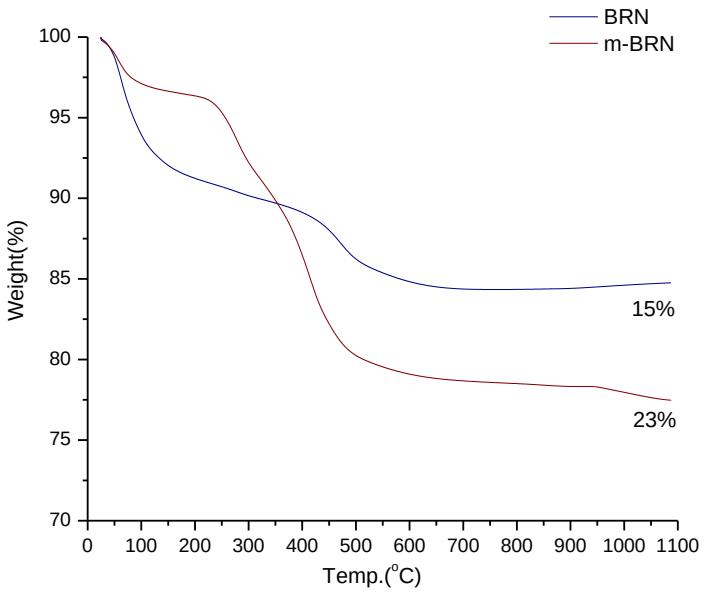

Figure 4.13 TG curves of BRN and m-BRN (<2μm).

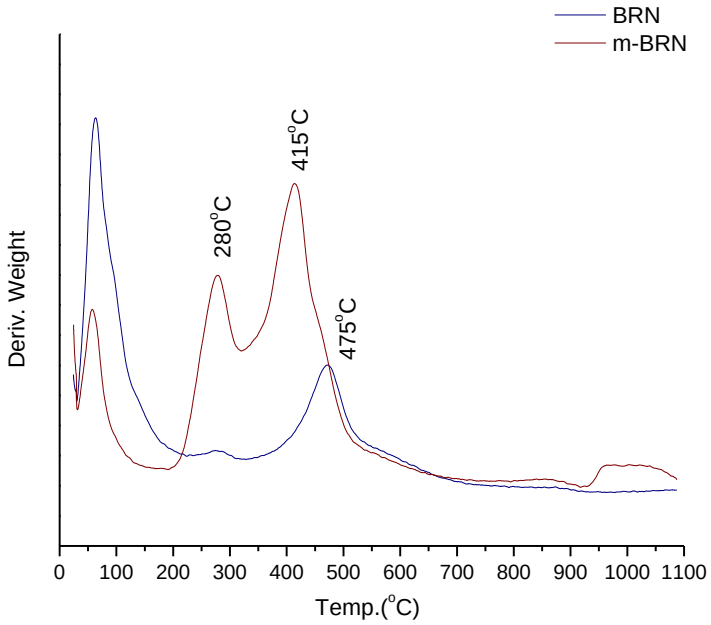

Figure 4.14 DTG curves of BRN and m-BRN (<2μm).

In order to analyze the thermal effects of the m-MMT inside the PLA nanocomposite, analysis of the three different concentrations of m-MMT/PLA and pure PLA was conducted by thermogravimetric analysis and the results are shown as Figure 4.15 and Table 4.2. The results show that with a higher percentage of m-MMT within the nanocomposite, the temperature required for 5% and 50% decomposition is increased. According to Wu, T. -M. & Wu, C. -Y. (2006) and Liu *et al.* (2011) organo-montmorillonite introduced into the PLA system might enhance the thermal stability of the nanocomposites due to the presence of inorganic layered silicates and a better interaction between m-MMT and PLA in the fabricated nanocomposites. In Figure 4.16, the DTG curves show that the pure polylactide and the nanocomposites have endothermic signals starting at temperatures related to the amount of organo-clay. In Figure 4.12, the loss of alkylammonium within the modified montmorillonite is at 313 ^{o}C and 424 ^{o}C. However, since the amount of m-MMT within the nanocomposites are only 3%, 5% and 8%, the loss of the alkylammonium which is located on the exterior of the clay layer, at around 313 ^{o}C, is not obviously shown in the curve and forms the shoulder of the peak at 357 ^{o}C. The loss of the alkylammonium which interacts electrostatically with the clay surface, at around 424 ^{o}C, is not shown in Figure 4.15; this might be due to the substitution of the PLA, and can also prove the intercalation of the PLA. The loss of PLA is around 357 ^{o}C, and after this

decomposition, the weight left over is proportional to the 3%, 5% and 8% of montmorillonite.

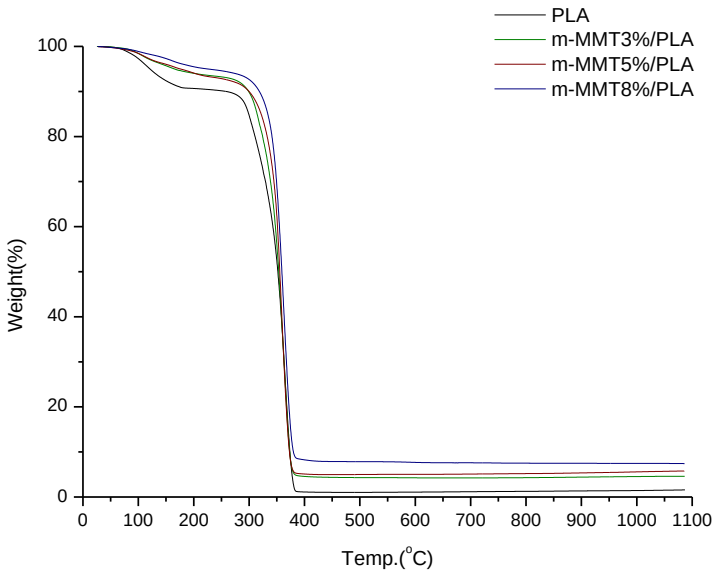

Figure 4.15 TG curves of pure PLA and different concentration of m-MMT/PLA.

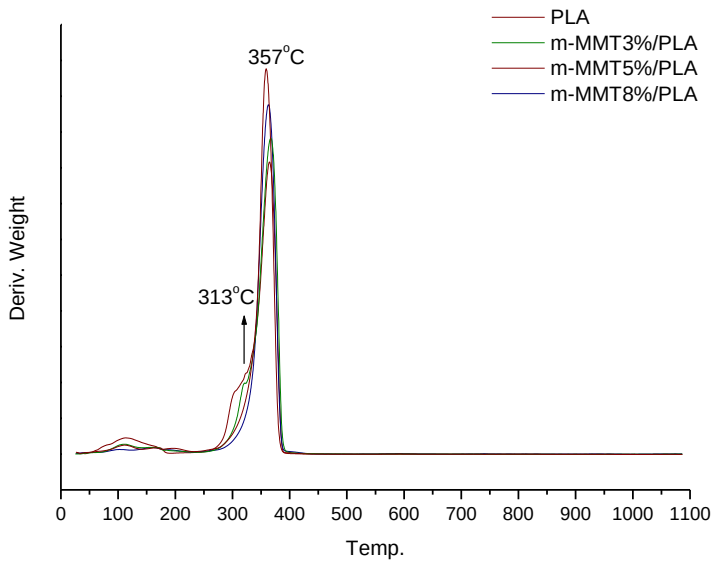

Figure 4.16 DTG curves of pure PLA and different concentration of m-MMT/PLA.

	PLA	m-MMT3%/PLA	m-MMT5%/PLA	m-MMT8%/PLA
T_{-5}	121°C	165°C	176°C	225°C
T_{-50}	352°C	353°C	355°C	359°C

Table 4.2 5% weight loss (T-5) and 50% weight loss (T-50) temperature of PLA and three different concentrations of m-MMT/PLA.

Porosimetry

The nitrogen isotherm (Fig 4.17) and the values analyzed by Brunauer–Emmett–Teller (BET) (Brunauer *et al*., 1938), Barrett-Joyner-Halenda (BJH) and T-plot methods (Lippens & de Boer, 1965) (Table 4.3) identify the effects of the CTA- ion exchange on the pore structure, surface nature, and adsorption properties of MMT (<2µm) and BRN in silt-clay fraction (<63µm) and clay fraction (<2µm). The main change is that the monolayer capacity and the BET surface areas decreased but the pore diameters increased in every sample after its modification by CTA-ions. The BET surface area could be increased or decreased depending on the arrangement of the surfactant. In this case, CTA-ions are large cations which act as pillars to expand the interlayer of clay and increase pore diameters but compactly pack the interlayer and block the nitrogen molecules from the pores, decreasing the surface and micropore areas (Wang *et al*., 2004; Lee *et al*., 1999; Xi *et al*., 2010). The micropores and mesopores are formed in the interlayers. As shown in Figure 4.17(a), (b), the nitrogen isotherm of BRNs have an obvious round knee at low pressure, indicating a micropore filling process. For all nitrogen isotherms, at higher pressure, the multilayer adsorption is exhibited representing the presence of mesoporosity. All desorption isotherms that have the hysteresis loops on the intermediate pressure show the capillary condensation on mesopores and macropores. The difference in the surface

area between silt-clay fraction and clay fraction of BRN is caused by the particle size (Veniale *et al*., 2007). In comparison between BRN and MMT, BRN has a larger surface area than MMT due to the illite content which was shown to have a positive relation with the specific surface area (Rebelo *et al*., 2010).

	BET surface area (m^2/g)	T-plot micropore area (m^2/g)	BJH average pore diameter(Å)
BRN <63μm	38.5	18.3	78.0
m-BRN <63μm	6.83	-	159
BRN<2μm	53.6	32.6	80.4
m-BRN<2μm	35.3	-	122
MMT<2μm	36.3	13.2	104
m-MMT<2μm	27.3	2.02	195

Table 4.3 The porosimetry analysis values of samples.

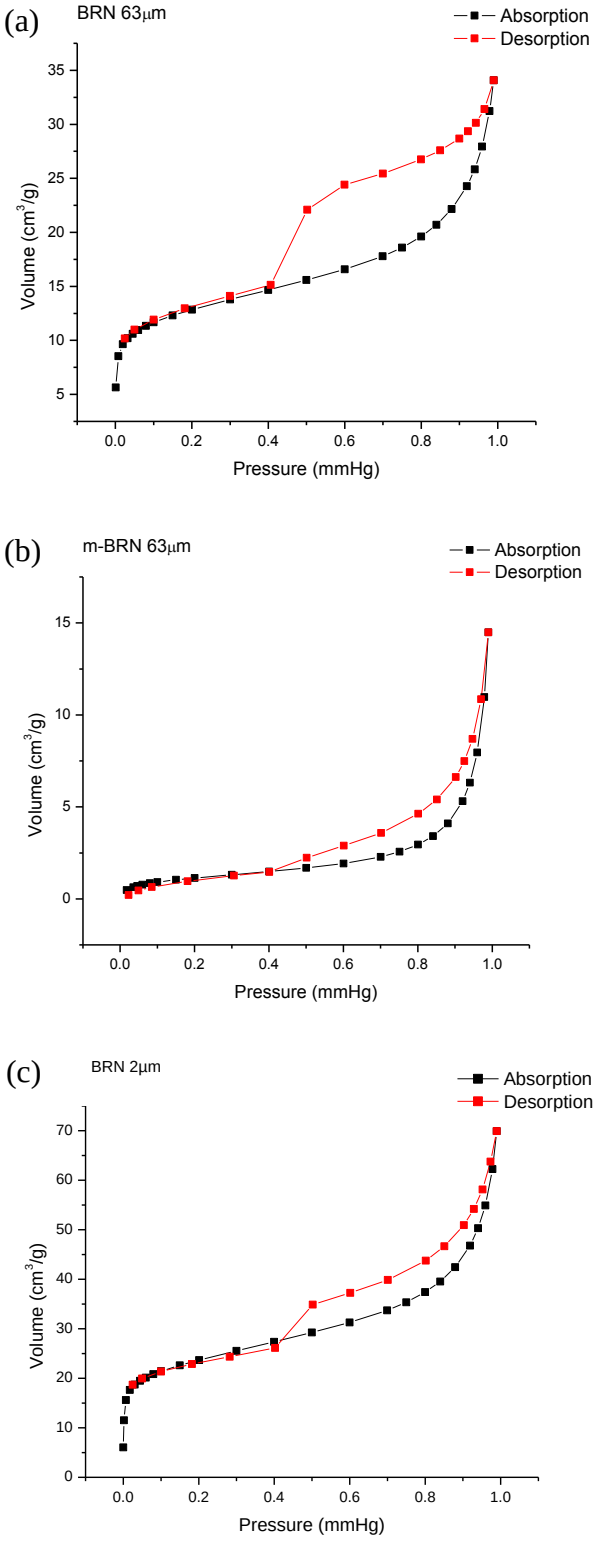

Figure 4.17 (a-c) The isotherm curves of BRN (<63 µm), m-BRN (<63 µm) and BRN (<2 µm).

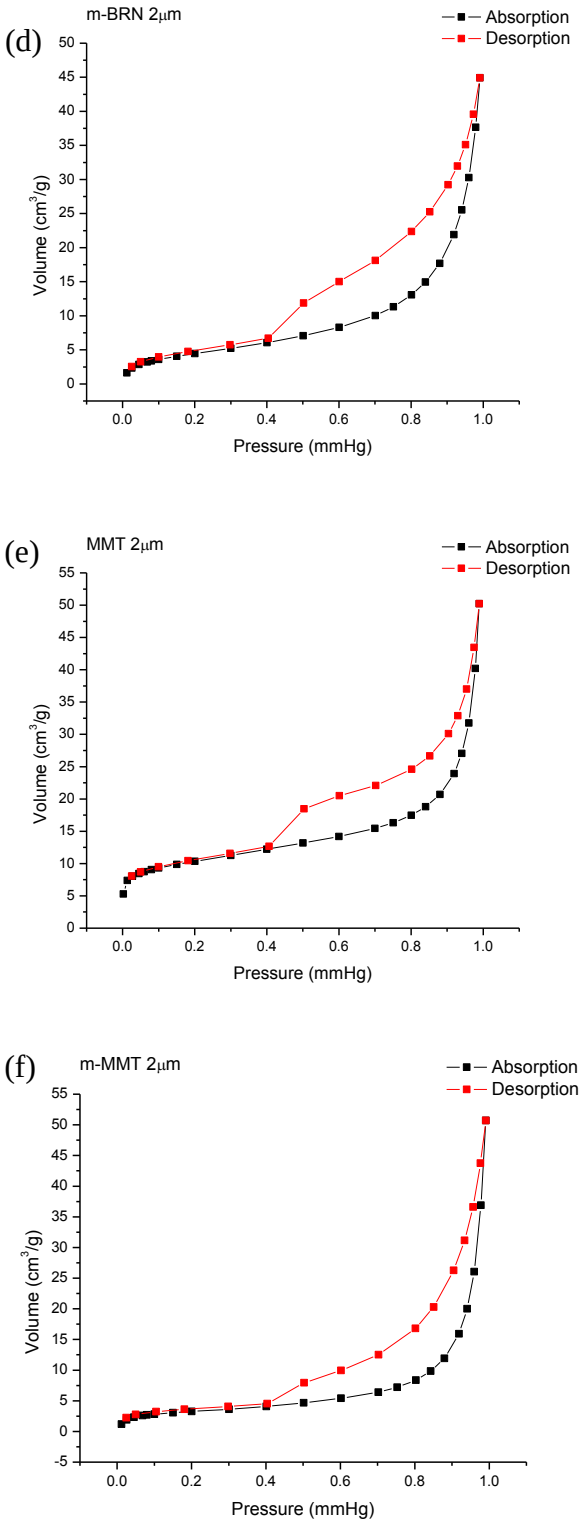

Figure 4.17 (d-f) The isotherm curves of m-BRN (<2μm), MMT (<2 μm) and m-MMT (<2 μm).

Infrared analysis (IR)

IR was used to identify the functional groups present on the surface (Fig 4.18). Compared to the raw montmorillonite (MMT) and Portuguese clay (BRN), there are some additional IR bands indicating the presence of the alkylammonium groups in the organo-clays m-MMT and m-BRN. The absorption bands around 2925 and 2850 cm^{-1} respectively correspond to asymmetric and symmetric vibrations of CH_2- groups from the alkyl chains. The intense absorption band at around 1470 cm^{-1} is associated with the C-H symmetric bending of (N^+)-CH_3 groups from alkylammonium (Fatimah & Huda, 2013). The two IR bands observed around 3630 and 910 cm^{-1} in all samples can be respectively assigned to the stretching and deformation vibration of hydroxyls in the [AlAl-OH] species which are also typical of dioctahedral smectites (Letaïef *et al.*, 2003). In the case of the location of Fe(III) in the tetrahedral environment, the stretching vibration bands of SiO are around 1010 cm^{-1}. The IR absorptions around 800 cm^{-1} could be attributed to deformation vibration of hydroxyls in [Fe(III)Fe(III)-OH] and [Fe(III)Mg-OH] (Letaïef *et al.*, 2003). The IR bands around 1630 cm^{-1} refer to the bending vibration of physically adsorbed water molecules of the interlayer (Mishra *et al.*, 2012). The bands around 3695 cm^{-1} and 695 cm^{-1} are characteristic of kaolinite which is only present in the BRN and m-BRN samples (Letaïef *et al.*, 2003).

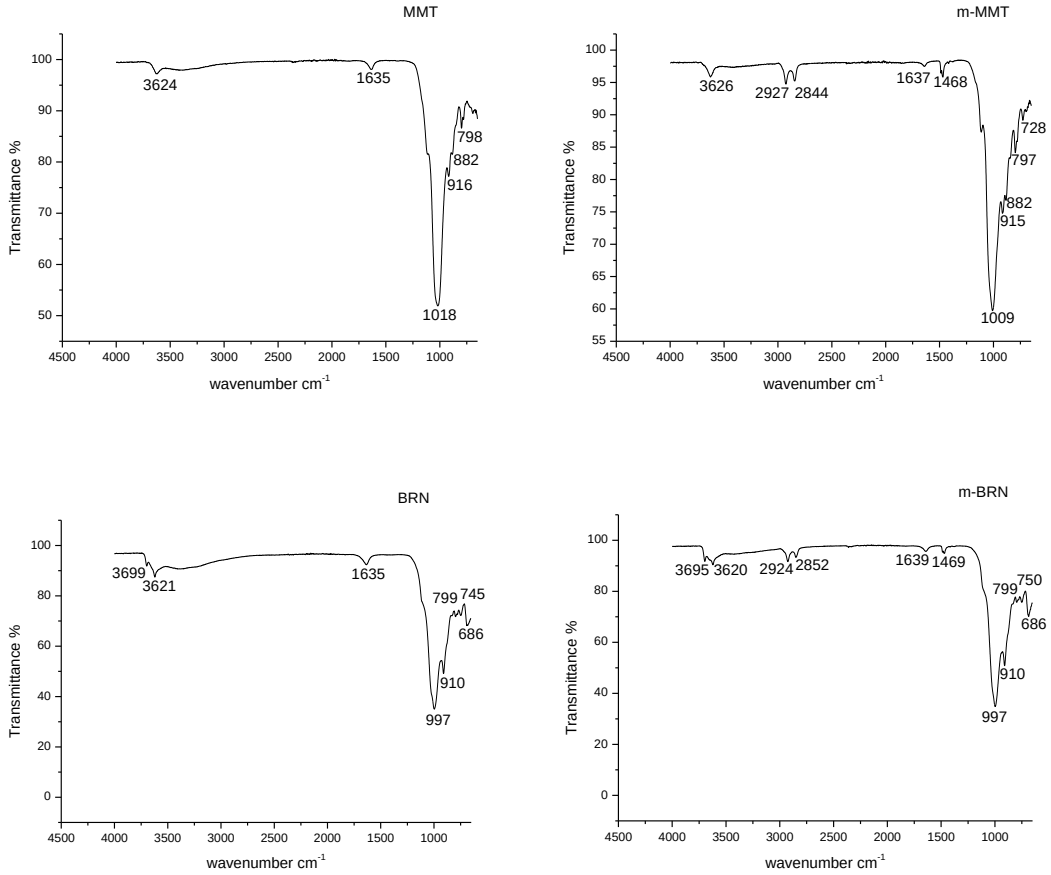

Figure 4.18 Infrared spectra of MMT, m-MMT, BRN and m-BRN.

Nuclear magnetic resonance (NMR)

In order to analyze the interactions of the CTA ions within various environments, an NMR analysis of CTAB, m-MMT, and m-MMT8%/PLA was performed. The result of ^{13}C CP/MAS of CTAB was shown as Figure 4.19. The signal at 63.7 ppm is assigned to C-1, at 55.4 ppm to methyl groups bonded to N, at 34.8ppm to C-14, at 32.7ppm to C-4~C-13, at 29.8 ppm to C-3, at 24.7 ppm to C-2, at 24 ppm to C-15, and at 16.8 ppm to C-16 (Theng *et al.*, 1998; Canet *et al.*, 1987). The signals for CTA ions in MMT (Fig 4.21) and BRN (Fig 4.20) are distinctly broader than those of their counterpart in the bromide salt. This is consistent with a more disordered structure in the CTA modified complex. The chemical shift at 32.1 ppm, assigned to -(CH_2)n- for CTA in the complex, is close to the corresponding value for CTAB. This suggests that the polymethylene chains of CTA in the interlayer complex are essentially extended in an all-trans zig-zag conformation as in the solid CTAB (Theng *et al.*, 1998). The signal due to N-methyl carbon at 55.4 ppm for CTAB is shifted to 54.6 ppm in m-MMT and 54.8 ppm in m-BRN respectively. These displacements may be due to changes in the electrostatic interactions between the cationic ‘heads’ of CTA and the negatively charged sites on the clay (Theng *et al.*, 1998).

For the characterization of PLA with MMT mixture, ^{13}C CP/MAS spectrum of m-MMT8%/PLA is shown in Figure 4.22. The spectrum exhibits three well-defined

bands located at 17.5, 70.4, and 171.6 ppm. Those peaks can be assigned respectively to carbons belonging to CH_3 group, CH group and C=O group of the PLA's repeating unit (Bernard & Chisholm, 2012; Gaurava, 2012; Bourbigot *et al.*, 2011). The spinning side bands (ssb) were measured at a distance of 4500Hz from the three main peaks. Although the signal is small, the peak representing CTA within the complex might be at 30 ppm. According to Theng *et al.* (1998), the displacement may largely be due to a change from an all-trans to a disordered conformation.

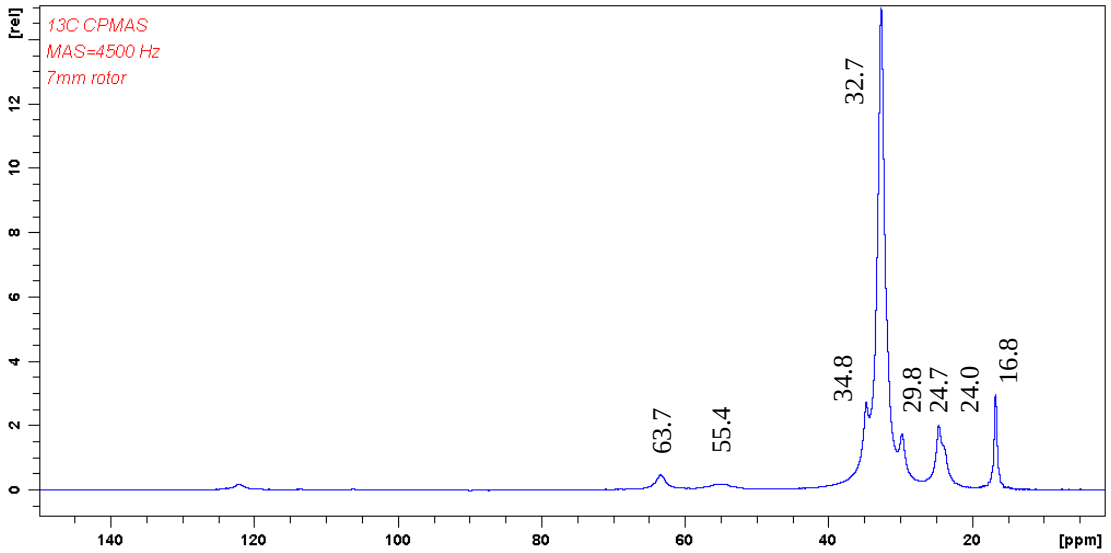

Figure 4.19 ^{13}C CP/MAS NMR spectrum of CTAB.

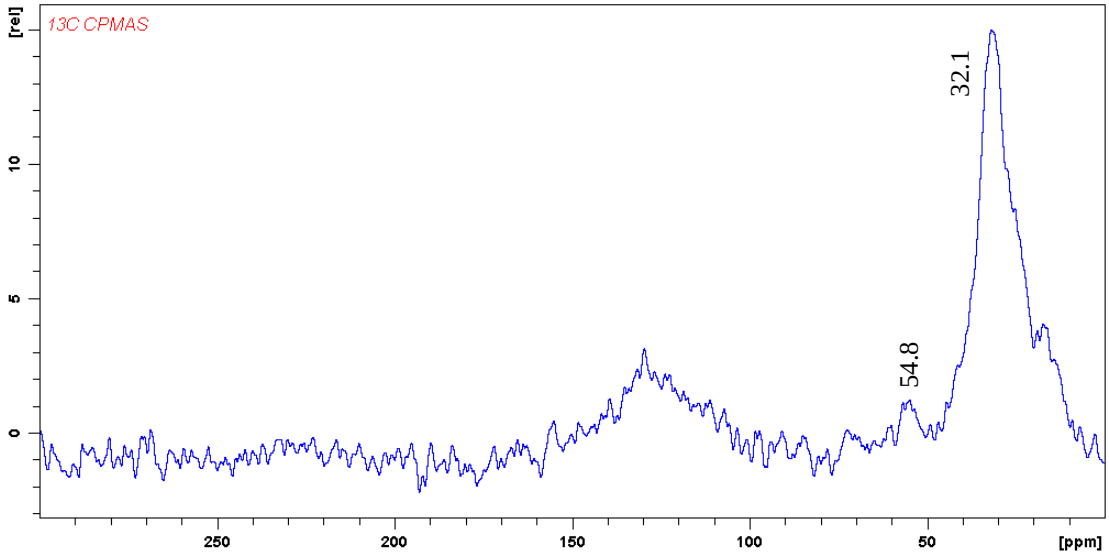

Figure 4.20 ^{13}C CP/MAS NMR spectrum of m-BRN.

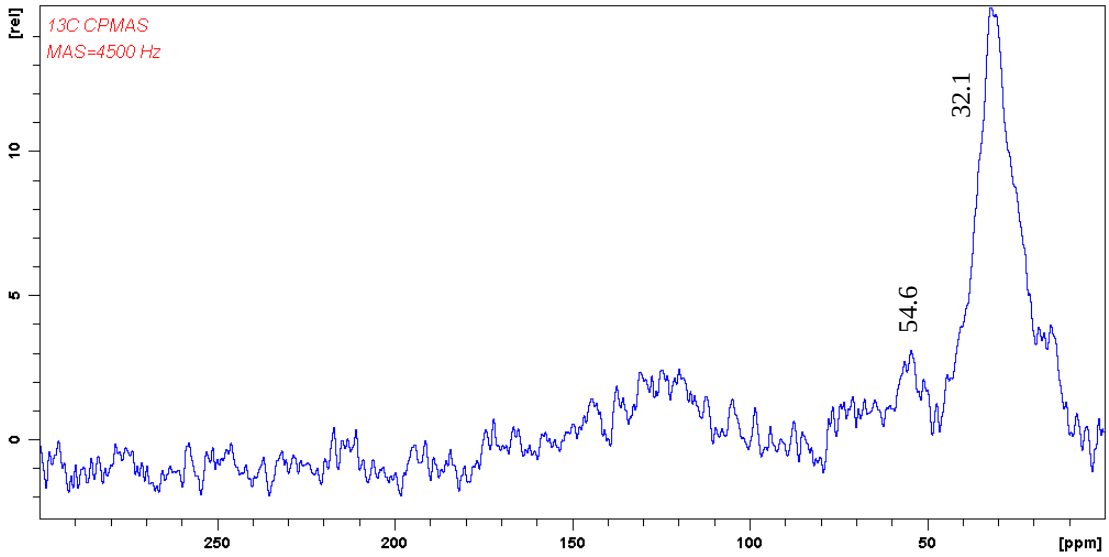

Figure 4.21 ^{13}C CP/MAS NMR spectrum of m-MMT.

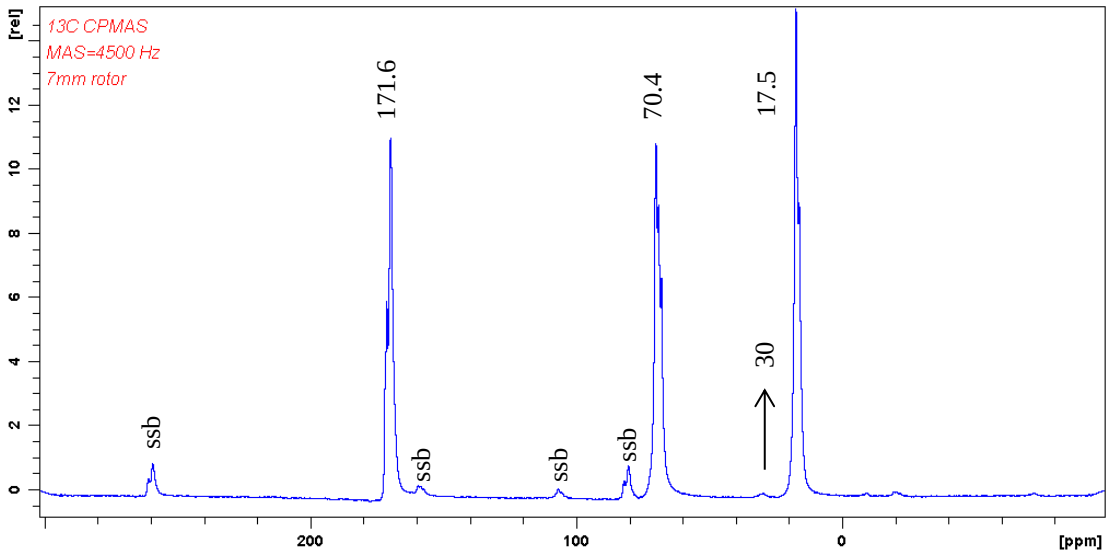

Figure 4.22 ^{13}C CP/MAS NMR spectrum of m-MMT8%/PLA.

Conclusion

Polylactide (PLA) nanocomposites with both the Portuguese sample (BRN) and montmorillonite (MMT) have been successfully prepared through the solution casting method with ultrasonic stirring using cetyltrimethylammonium bromide (CTAB) as the surfactant. The possibility of an exfoliated structure present in samples m-MMT3%/PLA, m-MMT5%/PLA, m-BRN3%/PLA, m-BRN5%/PLA and m-BRN8%/PLA is shown in XRD patterns where the basal spacing peaks are missing; results should be confirmed by transmission electron microscopy in future work. The m-MMT8%/PLA shows the different interlayer space of the nanocomposites on the TEM micrograph which is consistent with the broadened peak on the XRD pattern. Thermogravimetric analysis indicates the successful CTAB modification in the organo-clay m-MMT and m-BRN, and also shows an increased thermal stability of m-MMT/PLA nanocomposites compared to neat PLA. IR analysis shows the different absorption bands between the clay and the organo-clay and between MMT and BRN. NMR shows the small shift of the CH_2 peak of CTA in both organo-clay and PLA indicating the different conformations within the interlayer. The porosimetry results imply that the CTA ions inside the organo-clay decrease the nitrogen molecule adsorption but expand the interlayer spacing. With the confirmation of

nanocomposites synthesis, mechanical properties, heat distortion temperature and gas barrier properties could be conducted to compare with pristine PLA in a future work.

Reference

Bernard, A. & Chisholm, M. H. (2012). Synthesis of core–shell (nano) particles involving TiO_2, SiO_2, Al_2O_3 and polylactide. *Polyhedron, 46*, 1-7.

Bourbigot, S., Fontaine, G., Gallos, A. & Bellayer, S. (2011). Reactive extrusion of PLA and of PLA/carbon nanotubes nanocomposite: processing, characterization and flame retardancy. *Polym. Adv. Technol.,22*(1), 30-37.

Brunauer, S., Emmett, P.H. & Teller, E. (1938). Adsorption of Gases in Multimolecular Layers. *Journal of the American Chemical Society, 60* (2), 309-319.

Canet, D., Brondeau, J., Boubel, J. C. & Retournard, A. (1987). A one-dimensional selective version of the INADEQUATE experiment for determining carbon—carbon connectivities. Analysis of multi-pulse experiments by a vectorial representation. *Magnetic Resonance in Chemistry, 25*(9), 798-803.

Carrado, K. A., Decarreau, A., Petit, S., Bergaya, F., & Lagaly, G. (2006). Synthetic clay minerals and purification of natural clays. In F. Bergaya, B. K. G. Theng & G. Lagaly (Eds.), Handbook of Clay Science (pp.115-139). Amsterdam: Elsevier.

de Paiva, L.B., Morales, A.R. & Valenzuela Díaz, F. R. (2008). Organoclays: Properties, preparation and applications. *Applied Clay Science, 42*, 8–24.

Fatimah, I. & Huda, T. (2013). Preparation of cetyltrimethylammonium intercalated

Indonesian montmorillonite for adsorption of toluene. *Applied Clay Science, 74*, 115-120.

Gaurava, S., Ankita, M. & Pradeep, S. (2012). Characterization and In Vitro degradation studies of Synthesized Polylactide (PLA). *Research Journal of Chemistry and Environment,16*(2), 14-21.

Hoidy, W. H., Mansor, B., Ahmad, E. A., Jaffar Al Mulla, E. A. & Ibrahim, N. A. B. (2009). Synthesis and characterization of organoclay from sodium montmorillonite and fatty hydroxamic acids. *American Journal of Applied Sciences, 6*(8), 1567-1572.

Hrachova, J., Billik, P., & Fajnor, V. S. (2010). Influence of organic surfactants on structural stability of mechanochemically treated bentonite. *Journal of Thermal Analysis and Calorimetry, 101*, 161-168.

Krikorian, V. & Pochan, D. J. (2003). Poly (L-Lactic Acid)/Layered Silicate Nanocomposite: Fabrication, Characterization, and Properties. *Chemistry of Materials, 15* (22), 4317-4324.

Lagaly, G., Ogawa, M. & Dekany, I. (2006). Clay mineral organic interactions. In F. Bergaya, B. K. G. Theng & G. Lagaly (Eds.), Handbook of Clay Science (pp. 309-377). Amsterdam: Elsevier.

Letaïef, S., Casal, C., Aranda, P., Martín-Luengo, M.A. & Ruiz-Hitzky, E. (2003).

Fe-containing pillared clays as catalysts for phenol hydroxylation. *Applied Clay Science 22* (6), 263-277.

Lee, J.-F., Lee, C.-K. & Juang, L.-C. (1999). Size Effects of Exchange Cation on the Pore Structure and Surface Fractality of Montmorillonite. *Journal of Colloid and Interface Science, 217*, 172–176.

Lippens, B.C. & de Boer, J.H. (1965). Studies on pore systems in catalysts. V. The t method. *Journal of Catalysis, 4* (3), 319-323.

Liu, M.-T., Pu, M.-F., Ma, H.-W., Hu, Y.-F., Liu, X.-J. & Pang, X. (2011). The effect of organic modifier-12-aminolauric acid on morphology and thermal properties of polylactide nanocomposites. *Polymer Composites 32* (6), 1002-1008.

Maiti, P., Yamada, K., Okamoto, M., Ueda, K. & Okamoto, K. (2002). New polylactide/layered silicate nanocomposites: Role of organoclays. *Chemistry of Materials, 14*(11), 4654-4661.

Martín, Z., Jiménez, I., Gómez, M.A., Ade, H.W., Kilcoyne, D.A. & Hernádez-Cruz, D. (2009). Spectromicroscopy study of intercalation and exfoliation in polypropylene/montmorillonite nanocomposites. *Journal of Physical Chemistry B, 113* (32), 11160-11165.

Mishra, A.K., Allauddin, S., Narayan, R., Aminabhavi, T.M. & Raju, K.V.S.N.

(2012). Characterization of surface-modified montmorillonite nanocomposites. *Ceramics International, 38* (2), 929-934.

Ogata, N., Jimenez, G., Kawai, H. & Ogihara, T. (1997). Structure and thermal/mechanical properties of poly(/-lactide)-clay blend. *J. Polym. Sci. Part B: Polym. Phys.,35* (2), 389-396.

Ogawa, M., Wada, T., & Kuroda, K. (1995). Intercalation of pyrene into alkylammonium-exchanged swelling layered silicates: The effects of the arrangements of the interlayer alkylammonium ions on the states of adsorbates. *Langmuir, 11*(11), 4598-4600.

Pluta, M. (2006). Melt compounding of polylactide/organoclay: Structure and properties of nanocomposites. *Journal of Polymer Science, Part B: Polymer Physics, 44*(23), 3392-3405.

Ramirez, S., Righi, D., & Petit, S. (2005). Alteration of smectites induced by hydrolytic exchange. *Clay Minerals, 40*(1), 15-24.

Ray, S. S. & Bousmina, M. (2005). Biodegradable polymers and their layered silicate nanocomposites: In greening the 21st century materials world. *Progress in Materials Science, 50* (8), 962-1079.

Ray, S. S., Maiti, P., Okamoto, M., Yamada, K. & Ueda, K. (2002). New polylactide/layered silicate nanocomposites. 1. Preparation, characterization, and

properties. *Macromolecules, 35*(8), 3104-3110.

Rebelo, M., Rocha, F. & Da Silva, E. F. (2010). Mineralogical and Pysicochemical characterization of selected Portuguese Mesozoic-Cenozoic muddy/clayey raw materials to be potentially used as healing clays. *Clay Minerals, 45*(2), 229 – 240.

Ruiz-Hitzky, E., Darder, M., & Aranda, P. (2005). Functional biopolymer nanocomposites based on layered solids. *Journal of Materials Chemistry, 15*(35-36), 3650-3662.

Tenn, N., Follain, N., Soulestin, J., Crétois, R., Bourbigot, S. & Marais, S. (2013). Effect of nanoclay hydration on barrier properties of PLA/montmorillonite based nanocomposites. *Journal of Physical Chemistry C, 117*(23), 12117-12135.

Theng, B. K. G., Newman, R. H., & Whitton, J. S. (1998). Characterization of an alkylammonium-montmorillonite-phenanthrene intercalation complex by carbon -13 nuclear magnetic resonance spectroscopy. *Clay Minerals, 33*(2-3), 221-229.

Veniale, F., Bettero, A., Jobstraibizer, P. G. & Setti, M. (2007).Thermal muds: Perspectives of innovations. *Applied Clay Science, 36*, 141–147.

Wang, C.-C., Juang, L.-C., Lee, C.-K., Hsu, T.-C., Lee, J.-F. & Chao, H.-P. (2004). *Journal of Colloid and Interface Science, 280* (1), 27–35.

Wu, T. -M. & Wu, C. -Y. (2006). Biodegradable poly(lactic acid)/chitosan-modified

montmorillonite nanocomposites: Preparation and characterization. *Polymer Degradation and Stability, 91* (9), 2198-2204.

Xi, Y., Martens, W., He, H., & Frost, R. L. (2005). Thermogravimetric analysis of organoclays intercalated with the surfactant octadecyltrimethylammonium bromide. *Journal of Thermal Analysis and Calorimetry, 81*(1), 91-97.

Xi, Y., Mallavarapu, M. & Naidu, R. (2010). Preparation, characterization of surfactants modified clay minerals and nitrate adsorption. *Applied Clay Science, 48*, 92–96.

Xie, W., Gao, Z., Pan, W., Huner, D., Singh, A., & Vaia, R. (2001). Thermal degradation chemistry of alkyl quaternary ammonium montmorillonite. *Chemistry of Materials, 13*(9), 2979-2990.

General Conclusions

For the first part, in order to study the Portuguese raw sample BRN's use for pharmaceutical applications, several methods of characterization was performed. Generally, the properties of BRN are dominated by smectite and are less affected by illite, kaolinite and other minerals. The particle size, pH, cation exchange capacity, swelling potential, abrasivity and cooling rate are applicable for therapeutic applications such as cataplasms and mud baths. However, the amount of As and Pb are slightly over the criterion of "Permitted Daily Exposure". Therefore, advanced bio-availability examinations should be done to ensure safety when applied for topical and oral purposes.

For the second part, in order to increase the properties of polylactide, an attractive polymer nowadays, BRN and SWy2 montmorillonite (MMT) were modified by CTAB and blended with polylactide forming nanocomposites using the solution casting method. The level of dispersion was assessed by XRD and TEM. The characterization of neat and CTA modified clays were carried out by TGA, porosimetry, IR and NMR. The addition of organo-clays within the complexes improved the thermal stability of PLA. The different conformations of CTA-ions within the complex were revealed by NMR. The exfoliations of several organo-clay/PLA nanocomposites were initially proven by XRD. Since this

experiment is the preliminary test, the advanced confirmation of the exfoliated structure for other nanocomposite samples should be done in a future work.

Overall, the synthesis of the nanocomposites was successfully prepared. The further properties could be measured such as mechanical and thermal properties. With the elimination of hazardous elements, the BRN/PLA nanocomposites could be applied on the medical implants, packaging and containers.